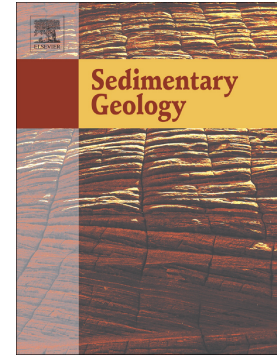# Journal Pre-proof

Seismic stratigraphy and sediment cores reveal lake-level fluctuations in Lake Iznik (NW Turkey) over the past ~70 ka

R. Gastineau, F.S. Anselmetti, S.C. Fabbri, P. Sabatier, P. Roeser, S. Gündüz, M. Şahin, E. Duarte, W. Rapuc, A.C. Gebhardt, S.O. Franz, F. Niessen, J. de Sigoyer

Please cite this article as: R. Gastineau, F.S. Anselmetti, S.C. Fabbri, et al., Seismic stratigraphy and sediment cores reveal lake-level fluctuations in Lake Iznik (NW Turkey) over the past ~70 ka, *Sedimentary Geology* (2024), https://doi.org/10.1016/j.sedgeo.2024.106620

This is a PDF file of an article that has undergone enhancements after acceptance, such as the addition of a cover page and metadata, and formatting for readability, but it is not yet the definitive version of record. This version will undergo additional copyediting, typesetting and review before it is published in its final form, but we are providing this version to give early visibility of the article. Please note that, during the production process, errors may be discovered which could affect the content, and all legal disclaimers that apply to the journal pertain.

Seismic stratigraphy and sediment cores reveal lake-level fluctuations in Lake Iznik (NW Turkey) over the past ~ 70 ka.

R. Gastineau (1, 2)*, F.S. Anselmetti (3), S.C. Fabbri (3), P. Sabatier (1), P. Roeser (4), S. Gündüz (5), M. Şahin (5), E. Duarte (1, 2), W. Rapuc (1, 6), A.C. Gebhardt (7), S.O. Franz (4), F. Niessen (7), and J. de Sigoyer (2)

(1) EDYTEM, Université Savoie Mont-Blanc, CNRS, Le Bourget du Lac, France

(2) Univ. Grenoble Alpes, Univ. Savoie Mont Blanc, CNRS, IRD, IFSTTAR, ISTerre, 38000 Grenoble, France

(3) Institute of Geological Sciences and Oeschger Centre for Climate Change Research, University of Bern, Baltzerstrasse 1+3, 3012 Bern, Switzerland

(4) Environmental Geology Group, Institute of Geosciences, Bonn University, Nussallee 8, 53115 Bonn, Germany

(5) Bursa Uludağ Üniversitesi, Fen-Edebiyat Fakültesi, Arkeoloji Bölümü, Görükle, Bursa, Turkey

(6) Department of Earth Sciences, Durham University, Durham DH1 3LE, United Kingdom

(7) Alfred Wegener Institute (AWI) Helmholtz Centre for Polar and Marine Research, 27568 Bremerhaven, Germany

*Corresponding author: Renaldo Gastineau (renaldo.gastineau@univ-savoie.fr)

Abstract

Our study aims to understand the palaeohydrological history of Lake Iznik and unravel the complex interplay between climatic, tectonic, and environmental factors that have shaped this Turkish basin. Through the analysis of seismic stratigraphy and sediment cores, we reveal a significant lowstand, indicating a lake level 60 m lower than today at ~70 ka BP. Subsequently, a major phase of stepwise transgression is evidenced by 13 buried palaeoshorelines between ~70-45 ka BP. From 45 to ~10 ka cal BP, strong currents controlled the sedimentation in the lake, as evidenced by the occurrence of contourite drifts. Between ~14-10 ka cal. BP, a major lowstand indicating a drier climate interrupted the current-controlled sedimentation regime. From ~10 ka cal. BP, the subsequent increase in lake level occurred at the same time as the reconnection between the Mediterranean and Black Seas. Archaeological evidence, including submerged structures of a basilica, establishes a link between lake-level changes and human settlement during the last millennium. The level of Lake Iznik has since continued to fluctuate due to climate change, tectonic events, and human activity.

Keywords: Lake-level fluctuations, seismic stratigraphy, lake sediments, climate, palaeohydrology, human activities, tectonics

2

1   INTRODUCTION

Lakes provide essential ecosystem services to society, including irrigation of agricultural crops and recreational areas. Understanding past and future changes in lake levels is essential for human development, as these fluctuations can lead to population displacement due to rising or falling lake levels and affect water resources and human settlements. They also represent wildlife habitats for many species (e.g. Jenny et al., 2020; Özuluğ et al., 2005). These fluctuations, whether caused by rising water impacting settlements or acting as a limiting factor in water resource availability (e.g. Guédron et al., 2023), are often associated with climate change in closed basins. They respond to variations in the precipitation-to-evaporation ratio (P-E) across the watershed (Abbott and Anderson, 2009). Lake levels may also be influenced by tectonic factors, such as subsidence due to normal faulting (e.g. Lezzar and Tier, 2002), or by geomorphological processes, such as landslides affecting outlets or inlets in hydrologically open systems (e.g. Fouinat et al., 2018). Notably, human activities, such as water use for agriculture or industry, have induced significant lake-level variations globally over the last century (e.g. Ariztegui et al., 2010; Davraz et al., 2019), unless regulated by humans controlling the lake's outlet (e.g. Geyer et al., 2001).

Here, we investigate Lake Iznik, Turkey's fifth-largest lake. Our objective is to understand the various regional factors that have influenced the hydrological history of the lake for over 70 ka BP. More than 126000 people are living in the two largest cities on the lake shoreline i.e. Orhangazi and Iznik (www.nufusu.com: data from 2023) so that many people are affected by lake-level changes. The lake's hydrology is notably influenced by tectonics, particularly the middle strand of the North Anatolian Fault bordering the south of the lake (MNAF; e.g., Doğan et al., 2015; Gastineau et al., 2021; Öztürk et al., 2009). Coupled with a persistent human footprint dating back to 6,000-5,400 BCE (Miebach et al., 2016; Roodenberg, 2013), and climatic variations evidenced by a long-term reconstruction indicating intervals of deeper and shallower water depths since 31 cal. BP (Roeser et al., 2016), the environmental history of Lake Iznik appears complex. Recent discoveries, such as a dynamically fluctuating shoreline (e.g., Roeser, 2014) and the Basilica of St Neophytos dating from the fourth or fifth century CE (e.g. Şahin, 2014; **Fig. 1**), have raised numerous questions regarding long- or short-term lake-level variations in Lake Iznik. Based on high-resolution seismic stratigraphic data, sediment cores, and a comprehensive literature review, this study examines local climate patterns, tectonic activity, and the impact of human activities over the last 70 ka BP. The aim is to contribute to the global discussion on lake-level reconstructions and reveal the unique environmental history of Lake

Iznik within the Turkish landscape.

2 STUDY SITE

2.1 Lake settings

Lake Iznik has a maximum depth of ca. 70 m and is located in the southeastern extension of the Marmara Sea. It has a surface area of 298 km² and is located at ~83.5 metres above sea level (m.a.s.l.) (Gastineau et al., 2021). It extends N-S and E-W by 12 and 32 km, respectively (**Fig. 1b**). Five main rivers drain water from the catchment to the lake, while only a single output is present westwards (the Gölyatağı dere River), which drains water from the lake to the Marmara Sea (**Fig. 1b**). The modern lake has a salinity of ~0.5 to 1.0 mg L^{-1} (Roeser et al., 2016). The catchment, presenting a surface area of 1257 km², is relatively small compared to the lake's surface area. The climate in the catchment area is dominated by a Mediterranean pattern characterised by typical warm and dry summers and mild and moist winters, expressed by an inverse pattern between average in humidity and temperature (e.g. Köppen, 1900; Miebach et al., 2016; Ülgen et al., 2012).

Lake Iznik comprises three subbasins (**Fig. 1b**). One subbasin is isolated in the western part of the lake (WSB; maximum depth: ca. 45 m). An E–W elongated ridge at ~45 m depth separates the central part of the lake into two subbasins, a north-eastern sub-basin (NESB; max depth: ca. 55 m) and a south-eastern sub-basin (SESB; max depth: ca. 75 m). The SESB is delimited to the south by the MNAF, which has a normal component at this location and explains the deepest part of Lake Iznik (Doğan et al., 2015; Gastineau et al., 2021; Öztürk et al., 2009), and to the north by the Iznik Fault, which seems to have a mainly strike-slip component and small normal component, the fault currently has a vertical topographic step of ~1 m (Gastineau et al., 2021; **Fig. 1b**). The Iznik Fault's last rupture at the NESB's northern margin occurred at 1065 CE and showed a vertical offset of ~40 cm (Gastineau et al., 2021; **Fig. 1b**).

2.2 Previous studies of changes in lake level and water column depth

Lake-level variations in the Iznik Basin have already been described at different timescales by the study of (i) exposed and subaquatic palaeoshorelines, (ii) beach rocks, (iii) palaeoenvironment reconstructions, and (iv) submerged archaeological remains.

2.2.1 Exposed and subaquatic palaeoshorelines

Ikeda et al., (1991) first described at least three steps of wave-cut scarps along palaeoshorelines that

developed during highstands of the lake at 20-25 m, 65-80 m, and 115-125 m above the current lake level in the western part of the lake. Nevertheless, they argue that their elevations might have resulted from differential uplift in the basin due to the normal component of the MNAF south of the lake. However, no age was determined in that study. Benjelloun et al., (2021) described these three steps of wave-cut scarps as "terraces" at the lake's northern shore based on terrestrial field observations and dated them based on the in situ produced terrestrial cosmogenic nuclide (TCN) method providing exposure ages. The highest shoreline 1 (~110 m above lake level (a.l.l.)) crosscuts sediment dated to $27.0^{+10.9}_{-13.0}$ ka BP (**Fig. 1b**). The shoreline 2 (~60 m a.l.l) crosscuts sediment dated to $19.6^{+7.7}_{-7.2}$ ka BP, and the shoreline 3 (~20 m a.l.l.) crosscuts alluvial to deltaic deposits on the southern of the lake $3.8^{+6.3}_{-2.7}$ ka BP (denotes S1, S2 and S3 in **Fig. 1b**, respectively). Those sediment surfaces were characterised by previous high lake levels that were conserved due to tectonic uplift (Benjelloun, 2017). Using a high-resolution digital elevation model (DEM), the north-south orientation of these data measured from the palaeo-"terraces" demonstrates a gradual inclination towards the south, with the extent of the tilt increasing as the terrace age increases. This gradual tilting has been interpreted as the outcome of vertical movement along the MNAF along the lake's southern shoreline (Benjelloun, 2017; Ikeda et al., 1991).

In addition, a series of subaquatic palaeoshorelines were first described with seismic data (Öztürk et al., 2009) and then imaged with a multibeam bathymetry (Gastineau et al., 2021, 2023) at water depths of 44–46 m in the north and 45–48 m in the south; they were interpreted as indicators of past low lake levels; however, their specific ages remain undetermined.

2.2.2 **Beach rocks**

Most of the western and southern coasts of Lake Iznik contain beach rocks, indicating that the lithification processes of abandoned beach sediments occurred primarily due to the carbonate cement that formed along the shoreline (**Fig. 1b**) (e.g. Geyer et al., 2001). Erginal et al., (2012) studied beach rocks at the southern lakeshore. The beds are inclined lakewards, and samples were collected 5 to 40 cm below the current lake level. They were dated to between 20.285 ± 2.067 ka (Last Glacial Maximum: LGM) and $2.456 \pm 0.566.5$ ka using optically stimulated luminescence (OSL) (Erginal et al., 2012). Öztürk et al., (2016) analysed beach rocks at the same location and OSL-dated 33 samples at depths ranging from 5 to 80 cm below the current lake level. These authors found rather different results, showing that the beach rocks had been formed during four drier periods: the late Pleistocene (15-9 ka BP), Holocene climatic optimum (7.9-5.6 ka BP), middle/late

Holocene (4.9-2.8 ka BP), and late Holocene (2.0-0.9 ka BP) when the lake level was between +1 and -1 m above the present lake level. The authors argue that the consistency with the climate data confirms this finding (e.g. Ülgen et al., 2012).

2.2.3 Palaeoenvironmental reconstructions

Previous multiproxy investigations have shown that the carbonates preserved in the sediment column, combined with redox-sensitive proxies (Roeser et al., 2016) and vegetation reconstruction (Miebach et al., 2016), reflect the water depth at the time of sedimentation. Such reconstructions were performed based on the climate sensitivity of the carbonate precipitation (e.g. Ülgen et al., 2012; Viehberg et al., 2012) and the early diagenetic fingerprint at the sediment-water interface imposed by climate-controlled processes occurring in the water column of the lake (Roeser et al., 2016). In the long-term records, Roeser et al., (2016) have inferred a deeper water column during the LGM, with periods of ice coverage, and a shallower water column during the early Holocene, i.e. after the glacial period and up to 9 ka cal. BP, when large changes occurred and the basin was likely filled to levels close to those of today (Roeser et al., 2016), with marked fluctuations during the Holocene (Ülgen et al., 2012).

2.2.4 Archaeological remains

Various archaeological excavations suggest that farming began at 6000–5400 BCE in the watershed (Roodenberg, 2013), suggesting that the water resources in the basin were reachable and that the respective water quality was attractive for human settlements at this time (Miebach et al., 2016; Roeser et al., 2016). Iznik, formerly Nicaea, was an important city throughout Antiquity. Lake-level variations over the last two millennia have been investigated and are mainly linked to the degree of obstruction of the outlet by humans (Geyer et al., 2001). During a 2014 aerial photographic survey, the submerged St. Neophytos Basilica was discovered from the eastern shore of the lake at an average water depth of two metres (Şahin, 2014; Şahin and R. Fairchild, 2018; **Fig. 1c**). Erginal et al., (2021) proposed that the basilica had been flooded and destroyed by a rising lake level during the last 1500 years. Lake-level drops during recent years (e.g. Roeser, 2014, their appendix figures; **Fig. 1c**) expose the basilica, showing that the lake level can vary significantly even on short time scales. This decreasing trend from ~85 (2000) to 83 (2023) m above the sea level (a.s.l.) (Özen et al., 2014) is likely due to increased water use for agriculture combined with periods of intense drought (e.g. Davraz et al., 2019; Yagbasan et al., 2017).

3   DATA AND METHODS

3.1   Seismic data

A grid of 292 km of seismic reflection lines was acquired during two surveys in 2005 (127 km) and 2021 (165 km). The first grid (2005) was acquired using a 3.5 kHz system (Geopulse, Geoacoustic) with an array of four transducers that act as senders and receivers (Mod. TR-1075A, Massa, USA). The shot interval was one second, and the vessel's average speed was 5 km h^{-1}. All 3.5 kHz data were digitised in SEG-Y format (Octopus 360, Octopus Marine Systems, UK) and bandpass filtered (1,500 to 5,000 Hz) using Reflex software (Sandmeier Software, Germany). In 2021, seismic data were recorded with an identical system fixed on an inflatable catamaran and attached to the side of a fishing boat. The digital recording of the seismic data in SEG-Y format was carried out with the Coda Octopus DA4G-USB 500 system. The shot interval was 311 ms at an average vessel speed of 6-8 km h^{-1}. A Garmin GPS receiver with ~5 m accuracy and Fugawi navigation software (Northport Systems Inc., Toronto, Canada) guaranteed accurate positioning. Seismic data were processed with a bandpass filter (1.5-2.0 and 6.5-7.0 kHz).

The vertical resolution of both datasets is ~10 cm. All sections were interpreted using the IHS Markit® Kingdom Suite v.2018. Furthermore, a sound velocity of 1500 m s^{-1} was applied to perform a time-to-depth conversion and to estimate the depth and thickness of the different seismic sequences. It is important to note that 1500 m s^{-1} represents a minimum velocity for these sediments, as deposits with coarser grains, such as sand and gravel, would exhibit notably higher velocities. Consequently, the determined thicknesses can be considered minimal values.

3.2   Core studies

3.2.1   Sediment-core retrieval and core analysis

Gravity core IZN19_12 (N° IGSN TOAE0000000318), with a length of 119 cm, was recovered at 44 m of water depth from the NESB in April 2019 using a UWITEC gravity hammer corer (**Fig. 1b**). A long sediment core IZN21-IV (composite length 11.1 m, sampled at 40 m of water depth) and one pilot core (IZN21_05; length 42.5 cm) were collected with a UWITEC platform (EDYTEM/LSCE/C2FN) in November 2021 (N° IGSN CNRS0000023714). For the long sediment core, 3-m-long sections from three different holes were taken with a 1.5 m offset to ensure a sufficient overlap to provide a continuous record. Identifying specific layers on the overlapping sections combined with correlations of the XRF-core scanner signals allowed the

construction of an 11.1-m-long composite sediment sequence (**Fig. S1**) (hereafter called IZN21-IV). One gap occurs in the sequence from an approximately 7.965 to 8.165 m composite depth (mcd) between two sections where an overlapping section is missing.

In addition, we used chronological, geochemical, and grain-size data from the long cores collected from the ridge in the middle of Lake Iznik during 2009 in the frame of CRC-806: IZN09/LC1 (10 m), IZN09/LC2 (14 m) and IZN09/LC3 (14 m) (for more details on the methods applied on these cores, e.g. Itrax scanning or the sampling for dating, see Roeser et al. (2012); for the grain-size methodology and an updated age model, see Roeser et al. (2016)).

Hereafter, the analyses concern IZN19_12 and IZN21-IV only. Whole-core segments of IZN21-IV were scanned using a GEOTEK multisensor core logger to measure gamma-ray attenuation bulk density (d) and magnetic susceptibility (MS) at 5 mm resolution at the University of Bern. The sediment cores were then split lengthwise and photographed. The relative contents of major and trace elements were analysed with an X-ray fluorescence (XRF) Avaatech Core Scanner using a rhodium anode at EDYTEM Laboratory. The split-core surface was first covered with a 4-μm-thick Ultralene film to avoid contamination and desiccation of the sediment. Then, IZN19_12 was scanned at a resolution of 1 mm at 10 kV/200 μA for 15 s to detect Al, Si, S, K, Ca, and Ti and 30 kV/300 μA for 20 s to detect Mn, Fe, Ni, Cu, Zn, Br, Rb, Sr, Zr, and Pb (Richter et al., 2006). For the IZN21-IV Core, the measurements were performed at a resolution of 5 mm at 10kV/80 μA for 10 s for the first run and 30 kV/75 μA for 20 s for the second run. The geochemical data are ln-transformed to avoid matrix effects from grain size or water content (Weltje et al., 2015). A principal component analysis (PCA) was conducted on the geochemical results using R software version 3.5.1 (R Core Team, 2018) and the FactoMineR package (Lê et al., 2008) to explore potential correlations among the different measured elements and identify principal sediment end-members. The identification process involved determining the dimensions that explained the most variation in our data and then defining the correlations between different elements through geochemical end-members (e.g. Sabatier et al., 2010).

3.2.2 Chronology

Radiocarbon analyses of seven terrestrial organic plant macroremains were performed by accelerator mass spectrometry at the Poznan Radiocarbon Laboratory for Core IZN19_12. As part of Core IZN21-IV, eight radiocarbon analyses were performed on terrestrial organic plant macro remains and four were performed on bulk sediment by accelerator mass spectrometry at the LMC14 laboratory (CEA Saclay) and at LARA

8

laboratory (University of Bern) (see **Table 1** for details). [14]C ages were calibrated using the Intcal20 calibration curve (Reimer et al., 2020). The age models of cores IZN19_12 and IZN21-IV were calculated using the R code package *Bacon v.2.3.9.1* (Blaauw and Christen, 2011). This package applies a Bayesian approach for age-depth modelling for the entire distribution of the calibrated radiocarbon dates.

In addition, the occurrence of geochemically identified tephra allowed the age-depth model to be refined by comparison with the previously established history of volcanic ash deposition in the lake and its surroundings (Çağatay et al., 2015; Roeser et al., 2012) and to confirm the age model. For this purpose, thin sections of 8 cm long sedimentary slabs with tephra layers were polished, and the glass shards were geochemically characterised using a JEOL JXA-8230 electron probe X-ray micro analyser (EMPA; ISTerre Laboratory, University Grenoble Alpes) equipped with five wavelength-dispersive spectrometers (WDSs) and one EDS detector using a 15 kV voltage, 2 nA beam current, and 5–7 μm beam size. Three MPI-DING reference glasses (StHs6-80_G, Atho-G, and KE12-G) were analysed with the samples to verify analytical accuracy and exclude the loss of alkalis (Jochum et al., 2000, 2005, 2006; Metrich and Rutherford, 1992). The glass shards yielding a total oxide sum of less than 96%, were not considered in the interpretations, due to potential mineral impurities. The analytical data were normalised to 100% total oxide values for comparison.

4   RESULTS AND INTERPRETATION

4.1   Seismic sequences and seismic stratigraphy of the northern delta

Acoustic penetration of a maximum ~30 ms two-way travel time (TWT) (~20 m) allows the description of six seismic sequences (from the oldest Sequence VI to the youngest Sequence I) separated by unconformities and/or high-amplitude reflections (HARs) and/or seismic facies changes. In most cases, these sequences can be traced and correlated across the entire basin despite the presence of abundant gas blanking in the lake (**Figs. 2, 3**). In the following, time is always indicated as TWT.

- (VI) Sequence VI, which forms the acoustic basement of the present study, can be traced mainly to the northern shore of the lake. A transparent seismic facies characterises this seismic sequence and displays some truncated reflections at its upper boundary, eroded by the base of Sequence V (magenta HAR). These truncated reflections dip basinwards, similar to foresets of a prograding delta or shore foresets (**Figs. 2, 4**). In addition, three reflections become increasingly inclined as the depth of the stratigraphy increases (**Figs. 2d, 4b**), which could be the remnants of a prograding delta.

9

However, the base of the sequence is not visible, so only a minimum thickness of 10 ms (~7.5 m) can be estimated for this sequence.

- (V) This sequence has a uniform thickness of 8 ms (~6 m) and shows parallel internal reflections on the northern shore (**Figs. 2, 3a, b**). However, its base shows wavy features (**Fig. 4,** magenta HAR). A succession of mound-like wavy structures is particularly well developed in the easternmost profile on Sequence VI on both 3.5 kHz seismic sections on the lake's northern shore (**Fig. 4**). The shape of these features, commonly with a steep side facing the lake and a more gently dipping part facing the land, is typical for beach ridges marking palaeoshorelines that can develop only when the water level remains stable for some time (e.g. Anselmetti et al., 2009; Gilli et al., 2005). The lake level must rise quickly enough between the phases of beach-ridge formations so that the previously deposited shorelines are not directly eroded. The beach ridges were formed at the onset of Sequence V, with thirteen well-defined beach ridges forming a succession deposited directly on Sequence VI. They can be noticed at depths (including the water column) of 80 ms (60 m), 63 ms (47.25 m), 62 ms (46.5 m), 61 ms (45.75 m), 58 ms (43.5 m), 55 ms (41.25 m), 54 ms (40.5 m), 49 ms (36.75 m), 47 ms (35.25 m), 45 ms (33.75 m), 40 ms (30 m), 39 ms (29.25 m) and 36 ms (27 m) below the modern lake level. Such palaeoshorelines could have formed as the lake level decreased or increased. However, a decrease would have exposed them to weathering and heavy erosion. The observation shows well-preserved beach ridges here, likely indicating a stepwise increase in lake level upon initial transgression during Sequence V deposition. Along the lowermost palaeoshoreline at ~60 m depth, a basinal onlap marks the oldest Sequence V sediments (**Fig. 4a, b**). This feature is interpreted as the lowermost lake-level phase. This onlap occurs three metres below the lowermost palaeoshoreline, indicating the depth of the wave base lakeward of the palaeoshoreline, above which no lacustrine sediment (other than the shoreline itself) could accumulate. However, no evidence of onlaps below the other shorelines is observed, but such ridges form quickly (e.g. <100 years in Lake Michigan; Lichter, 1995) within a few years or decades. This time span might be too short to produce an onlap sufficiently thick to be recognised in our seismic data. Moreover, since one the lowermost beach ridge shows an increase in lake level, it seems very likely that the others do too, given that they are all observed on the same reflection (magenta HAR) and therefore share a common chronology.

10

- (IV) All reflections within Sequence IV are laterally continuous, with low-to-moderate amplitudes that downlap onto Sequence V toward the north (**Figs. 2, 3b, 4b**; dark green over orange HARs). In the NESB, this Sequence features prominent mound-like geometries with a maximum thickness of ~9 m toward the basin (**Fig. 3a, b**); thus, Sequence IV shows significant lateral variations in thickness at the basin scale. The mounds show many downlapping reflections at the base and internally, forming multiple unconformities (**Fig. 3a, b**). These downlaps usually wedge out toward zones where the thickness of Sequence IV is significantly reduced (**Fig. 3a, b**). We interpret these geometries as drift depositions induced by strong currents, as already described in other lacustrine (Gilli et al., 2005) or marine basins (Bashah et al., 2024). Thus, these downlaps cannot be interpreted as markers of lake-level variations, as they are directly linked to contourite drift and correspond to the thinning of the strata.

- (III) Sequence III is characterised by parallel, continuous, and medium-amplitude reflections. It extends across the entire basin. However, only its boundaries (HARs) are visible in the centre of the lake due to gas blanking (**Fig. 3c, d**). Sequence III partially laterally downlaps onto Sequence IV toward the north in **Figs. 2**, **3a, b**.

- (II) Sequence II exhibits more high-amplitude reflections with slightly chaotic facies. It is strongly confined in extent, and only the boundaries (HARs) are visible in the centre of the lake due to gas blanking (**Fig. 3c, d**). On the westernmost profile (**Fig. 2c**), only the base of Sequence II can be observed, and the upper part is eroded, with the reflections truncated. Additionally, in **Fig. 2b**, the base of Sequence II (light green HAR) displays an erosive discordance, truncating Sequences III, V, and VI. Both Sequences II and III present substantial lateral variations (E–W) (**Fig. 2**).

- (I) Sequence I is well-stratified with regular internal reflections except in the centre of the lake, where the gas prevents its observation (**Fig. 3c, d**). Its base (turquoise HAR) shows an erosive contact with the top of Sequences II and III (**Figs. 2, 3**). Northwards, on both seismic sections, the internal reflections of Sequence I are truncated at the inner edge of the underwater terraces described in section 2.2.1 (**Figs. 2, 3**). Sequence I onlaps its substrates (partially downlaps) before wedging out on the northern slope. It is absent on the steep slope (**Figs. 2, 3**).

4.2   Sediment records and their relationship with seismic data

11

4.2.1 Composite core IZN09/LC2&LC3

4.2.1.1 Description

Three long cores were retrieved in a previous study (Roeser et al., 2012) from different positions on the ridge in the lake's centre, and two of them were assembled into a composite profile (**Figs. 3c, d**). The composite core IZN09/LC2&LC3 (18 mcd) comprises five sedimentological units (**Fig. 5**), from top to bottom: (A) homogeneous, moderately organic, and black to greyish clayey silts with carbonates; (B) olive-grey carbonate mud rich in aragonite, with some diatoms; (C) silty clay matrix with carbonates, with a distinct iron monosulfide layer (sf2) at the top; (D) a clay matrix with the sporadic presence of shell fragments (these grading upwards), carbonate concretions, and detrital lithic fragments (dropstones); and (E) a silty clay matrix with carbonates, overprinted by monosulfide clusters (Roeser et al., 2016). This long composite core also contains two tephra layers: the Avellino tephra of Somma-Vesuvius/Italy and the Y2 tephra of the last glacial Santorini eruption (Roeser et al., 2012; Roeser et al., 2016).

4.2.1.2 Chronology and core-to-seismic correlation

Seismic-stratigraphic correlations throughout the lake basin allow us to establish i) a consistent link between the seismic pattern (seismic facies, seismic sequences) and the sedimentary units and ii) establish a robust chronologic framework by correlating the age models from the coring sites along the seismic stratigraphic horizons through the entire lake. The composite core IZN09/LC2&LC3 covers ca. 31 ka cal. BP (**Fig. 5b**; Roeser et al., 2016). To correlate the sediment core with the seismic data, we assumed a sound velocity of 1500 m/s in the water and the sediment (**Fig. 3d**). The turquoise and light green high-amplitude reflections (HARs), marking the transition between Sequences I/II and II/III, respectively, are correlated with core IZN09/LC2 at depths of 9 and 12.75 m below the lake floor (mblf), respectively (**Fig. 3d**; Roeser, 2014) and correspond to 10.25 and 14.1 metre composite depth (mcd) in the composite core IZN09/LC2&LC3, respectively (Roeser, 2014, their Table 3.1 and **Fig. 5b**). Therefore, the age model from Roeser et al. (2016) indicates an age of ~10 ka cal. BP and ~22 ka cal. BP, respectively for those HARs (**Fig. 5b**). Three other HARs, dark green, orange, and magenta, marking the transitions between Sequences III/IV, IV/V and V/VI, respectively, correlate to depths less than the 18 mcd of IZN09/LC2&LC3 and must therefore be older than ~31 ka cal. BP (**Figs. 3, 5b**). A constant sedimentation rate approximation from the bottom of the sediment core suggests that the dark green HAR may have an age of ~40 ka cal. BP (**Fig. 5b**).

4.2.2 Core IZN19_12

The sediment core IZN19_12 (119 cm) is located on the northeastern shore of the lake (**Figs. 3a, b**) and comprises two main sedimentary units (A and B), which are consistent with the macroscopic description of Roeser et al. (2012) (**Fig. 6a**). The sediment core crosses seismic Sequence I and the turquoise HAR. The base of the core reaches seismic Sequence III (**Figs. 3b, 6a**).

4.2.2.1 Description

Two units (A and B) are distinguished based on the macroscopic description (**Fig. 6a**), according to the description of a previous study (Roeser et al., 2012), in which we additionally distinguished four facies based on XRF data. The PCA applied to the sediment core identifies distinct end-members (**Fig. 6b**). Dimensions 1 and 2 (referred to as Dim 1 and Dim 2, respectively) account for 73.5% of the total variability, while Dimension 3 (Dim 3) explains 9.0% of the variability. Collectively, these three dimensions of the PCA explain 82.5% of the overall variability in the XRF signal (**Fig. 6b**). Four end-members were identified: (1) The first end-member displays high positive loadings on Dim 1 and intermediate to low positive loadings on Dim 2 and Dim 3, respectively (e.g. Al, Si, K, Ti, Rb, Zr, and Fe; dashed black and blue in **Fig. 6b**) and is denoted as "Terrigenous". (2) The second end-member, denoted as "Carbonates" displays high negative loadings on Dim 1 and intermediate positive loadings on Dim 2 and Dim 3 and comprises Sr and Ca (green in **Fig. 6b**). (3) The third end-member shows high positive loading in Dim 3, and comprises only Br (black in **Fig. 6b**) and is denoted as "organic matter". (4) The last end-member, "Redox", shows intermediate negative loadings on Dim 2 and Dim 3 and intermediate positive loadings on Dim 1 and comprises Mn and S (black in **Fig. 6b**)

Various geochemical ratios are then employed to characterise the sedimentary units and facies. (1) In Lake Iznik, the ln(Ca/Ti) ratio highlights the internal carbonate accumulation in the lake concerning detrital input, potentially exhibiting a grain-size dependency in coarse-grained sandy deposits. However, this ratio is source-dependent at the scale of the entire sedimentary sequence (Gastineau et al., 2023). (2) The ln(Mn/Fe) ratio serves as a reliable indicator of redox transitions in sediment records (e.g. Davies et al., 2015). (3) The ln(Br/Sr) ratio is used to emphasise lake productivity, given Br's association with organic matter in lake sediment (e.g. Davies et al., 2015; Lefebvre et al., 2021). (4) Additionally, the ln(Sr/Ca) ratio is employed to highlight lacustrine productivity linked to water depth. According to Roeser et al. (2016), Sr exhibits a strong correlation with aragonite, closely tied to endogenic calcium carbonate in Lake Iznik's water. For instance, a high aragonite accumulation can signify a shallow water column due to "a very 'thin' hypolimnion, i.e., a

13

short settling distance between the epilimnion and the sediment-water interface" (Roeser et al., 2016).

Sedimentary Unit 'A'

Positioned at the topmost part of the sediment core (from the top to ~85 cm depth), Unit A is decomposed by three distinct facies. 'A1', defined by light-brown silty clay, constitutes the background sedimentation. 'A2', characterised by intermittent event deposits with darker colours and fining upward grain size. These deposits exhibit low negative peaks of ln(Ca/Ti) and ln(Sr/Ca), suggesting a flood-induced origin rich in terrigenous carbonates, possibly calcite (Gastineau et al., 2023). 'A3', influenced by the fourth PCA end-member ("Redox"), this facies exhibits a coarse base with pebbles, indicative of a redox transition. The pebbles, which are angular, felsic and volcanic in origin (likely dacite), originate from the northern watershed (Eocene), and were transported by the Kurudere River (**Fig. 1b**). The overlying layers include a 2-cm-thick carbonate mud layer and brown, graded layers of oxidised sand to clay and finer dark brown sediments, indicating a substantial terrigenous input phase.

Sedimentary Unit 'B':

Positioned at the lowermost part of the sediment core (~85 cm to the core bottom at 110 cm), 'B' contains stiffer and more consolidated sediment at the core base that Facies 'A3' and contains many shell fragments. The XRF data and the light grey clay colour of the sediment indicate richness in carbonates (**Fig. 6a**), with the second PCA end-member, denoted as "Carbonates". Unit 'B' is characterised by a single facies, 'B1', and by a lower ln(Br/Sr) ratio (indicative of lower productivity) and a higher ln(Sr/Ca) ratio (suggesting a shallower water column compared to the top of the sediment core, *sensu* Roeser et al., 2016, **Fig. 6a**).

4.2.2.2 Chronology and core-to-seismic correlation

As part of its chronology, five organic terrestrial plant macroremains were dated from IZN19_12 (**Fig. 6c**). The sediment core IZN19_12 allows another independent age estimation of the turquoise HAR (**Figs. 3b, 6c**). The base of sedimentary Unit A above a coarse level characterising the turquoise HAR is dated to ~6.5 ka cal. BP (**Fig. 6c**). However, the seismic section at this site (44 m deep) indicates an unconformity across the turquoise HAR (**Fig. 3b**). Therefore, the age model results in a significant hiatus across this horizon, so the age of 6.5 ka cal. BP needs to be considered as the minimum age.

Core IZN19_12 spans at least 6.5 ka cal. BP and shows slight variations in the sedimentation rate (**Fig. 6c**): (1) A period with a low and constant (~0.05 mm yr^{-1}) sedimentation rate from 6.5 to 4 ka cal. BP; and (2) the sedimentation rate significantly increased from 4 ka cal. BP to the present day, reaching 0.3 mm yr^{-1}.

4.2.3 Master core IZN21-IV

Core IZN21-IV is located in the northwestern part of the lake (**Fig. 1b and Fig. 2d**). The composite core has a total length of ~11.1 m (**Fig. 7 and Fig. S1**). The sediment core crosses seismic Sequences I, II, III, and IV, i.e., all the HARs except the deepest magenta reflection (**Fig. 2d**)

4.2.3.1 <u>Description</u>

Six distinct sedimentary units have been identified primarily based on macroscopic descriptions (**Fig. 7a**). By applying PCA to the XRF data from core IZN21-IV, four distinct end-members were differentiated and found to be consistent with those found in core IZN19_12 (**Fig. S2**). The first two dimensions, Dim 1 and Dim 2, collectively account for 68.0% of the total observed variability. Dim 3, the third dimension, contributes an additional 8.8% to the overall variability.

Sedimentary Unit 'A'

Extending from 0 to 2 mcd, the uppermost sedimentary Unit 'A' is characterised by light-brown silty clay. This unit has been previously discussed in shorter cores (Gastineau et al., 2023). In contrast to the PCA of Core IZN19_12, in this case, Unit 'A' is influenced primarily by the organic and carbonate end-members rather than by the terrigenous one (**Fig. S2**).

Sedimentary Unit 'B'

This sedimentary unit consists of an olive-grey carbonate mud with low magnetic susceptibility, as described in Roeser et al. (2012) (referred to as Unit II). In Core IZN21-IV, this unit marks the transition just above the turquoise HAR, ranging from 2 to 2.2 mcd. Notably, in Core IZN19_12, Unit 'B' was situated below the turquoise HAR (**Fig. 6a**). The consistency of this unit in both cases indicates its deposition in shallow water, as the turquoise HAR serves as an emersion surface in both instances (**Figs. 2, 3**). The sediment is characterised by stiffness, maintains the same colour and contains shell fragments, thereby confirming its identity as Unit 'B' (**Fig. 7a**).

Within this 20-cm-thick unit, at 2.14 mcd, a two cm-thick black and surrounding clast of felsic volcanic origin (likely dacite) is observed, akin to what was identified in IZN19_12. The base of Unit 'B' is coarse and contains a layer of black sandy material resembling Facies 'A3' in Core IZN19_12 (**Fig. 6a**). This transition coincides with a density peak at 2 g.cm^{-3} and a shift in redox conditions, indicated by a high ln(Mn/Fe) ratio (**Fig. 7b, c**).

Sedimentary Unit 'C'

Between depths of 2.20 and 3 mcd, sedimentary Unit 'C' exhibits a consistent composition of olive-grey clay containing sporadic shells and shell fragments (bivalves) with low magnetic susceptibility (ca. 30×10^{-5} SI).

Sedimentary Unit 'D'

The transition to Unit 'D' (ranging from 3 to 5.2 mcd) aligns with the presence of the light green HAR (**Fig. 7a**). This unit is characterised by a silty clay matrix and the consistent presence of shells and shell fragments, identified as *Dreissena sp.* and other shell fragments from gastropods, as found in the glacial interval (Unit IV in Roeser et al., 2012). At the top of the unit, at a depth of 3 mcd, there is a distinct and sharp increase in magnetic susceptibility (from 20 to 80×10^{-5} SI). This increase is accompanied by a rise in the ln(Mn/Fe) ratio, attributed to the black coarse-grained tephra layer observed at a depth of 3.055 mcd.

Sedimentary Unit 'E'

In the depth interval of 5 to 6.2 mcd, sedimentary Unit 'E' displays the most variations in colour and grain size, incorporating sporadic sandy layers. This interval also features another two cm-thick black and subrounded felsic volcanic clast at 5.06 mcd and an additional tephra layer at 5.49 mcd. Facies 'E1' is characterised by a light grey and stiff silt, richer in terrigenous carbonates (lower ln(Sr/Ca) ratio). Facies 'E2' is a darker brown and stiff silt that is quite similar to E1 but enriched in organic matter (black patches) and endogenic carbonates with a higher ln(Sr/Ca) ratio and higher MS values ranging from 50 to 85×10^{-5} SI) compared to 'E1' (**Fig. 7a**). Both facies feature a few sandy layers (**Fig. 7a**).

Sedimentary Unit 'F'

Last, from 6.2 mcd to the base, sedimentary Unit 'F' is distinguished by lower magnetic susceptibility (approximately 40×10^{-5} SI) and homogeneous olive-grey silt containing substantial shells and shell fragments (bivalves).

4.2.3.2   Chronology and core-to-seismic correlation

The age-model for IZN21-IV was calculated with eight terrestrial plant macroremains, associated with four bulk and two tephra layers (**Table 1**). Two identified tephra layers could indeed be correlated to layers dated in cores from the Marmara Sea (e.g. Çağatay et al., 2015), which helped to refine the age model (**Fig. 7d**). The first tephra layer (3.055 mcd) is characterised by a heterogeneous, ~5-6-cm-thick, and irregular coarse ash layer containing abundant microcrystal-rich, high-vesicular micropumices with a phonolitic composition (**Fig. 8**). It has been geochemically correlated with the Cape Riva/Y2 eruption of Santorini, Greece and

therefore dated to 22 ka cal. BP and (Fenn et al., 2021; **Fig. 8a, b**). The observation of the Y2 tephra agrees with previous findings in the lake and supports the lithological correlation to the composite core IZN09/LC2&LC3 (Roeser et al., 2012). However, the Holocene Avellino tephra of the Somma-Vesuvius/Italy layer (3945 ± 10 cal. year BP; Sevink et al., 2011) has not been observed in the northern Core IZN21-IV, contrary to previous studies that have identified it in the lake (Gastineau et al., 2023; Roeser et al., 2012).

A second Pleistocene tephra layer found at 5.49 mcd in Core IZN21-IV is also defined by a heterogeneous, ~0.2-0.3 cm-thick and coarse ash layer. However, this layer differs from the uppermost tephra layer, as it contains abundant microcrystal-rich, high-vesicular micropumices predominantly of rhyolitic composition (**Fig. 8a**). It has been geochemically assigned to the Campanian Ignimbrite eruption/Y5, Italy (De Vivo et al., 2001), which has been dated to 39.2 ka cal. BP (Fenn et al., 2021; **Fig. 8a, c**).

However, the ages of organic terrestrial plant macroremains and bulk sediment raise significant questions because of their differences and inversions. The preference for bulk ages over terrestrial material ages is argued because (1) they have a low carbon content and (2) the presence of the Y5 tephra suggests ages older than 33 ka cal. BP below 5.49 mcd (**Fig. 7c** and **Table 1**).

In the final age model, Core IZN21-IV spans ~70 ka BP (**Fig. 7d**). Regarding the ages of the HAR, the age model of IZN21-IV allows for the assignment of ages to the turquoise HAR, with an estimated hiatus of ca. 15 ka, from ca. 20 to 4 ka cal. BP (**Fig. 7d**). This hiatus would explain the absence of any record of the Avellino tephra layer in this composite core. Regarding the other HARs in IZN21-IV, the light green HAR correlates to 22 ka cal. BP, corresponding to a tephra horizon; the dark green horizon at ~40 ka cal. BP, the orange HAR at ~45 ka cal. BP and a potential estimation suggest that the magenta HAR could be older than 70 ka BP (**Fig. 7d**). However, it is crucial to emphasise that the composite core IZN09/LC2&LC3, because of its sampling in the lake-central ridge structure, shows relatively continuous sedimentation, i.e. unaffected by the contourite currents such as the composite core IZN21-IV where contourite currents eroded part of the underlying sediment, which makes it possible to obtain a more accurate age model than from cores punctuated by hiatuses (e.g. Roeser 2014, their Figure 3.1; **Table 2**). The abovementioned HAR ages inferred based on the three sediment cores/composite sections presented in this study are summarised in **Table 2**.

5   DISCUSSION

The sedimentation pattern within a basin is driven mainly by the concept of accommodation space controlled

by i) particle input (terrestrial and endogenic), ii) water level (climate or inlet/outlet variation), and iii) tectonics (subsidence or uplift). Lake Iznik Basin shows an asymmetric (palaeo)bathymetry with deeper areas to the south and generally southwards-dipping layers (**Fig. 3c, d**). These geometries are typical of tectonically controlled lakes that form half-graben geometries in extensional strike-slip basins, such as some subbasins of the Marmara Sea (Seeber et al., 2010), other lakes such as Lake Van (Cukur et al., 2017) or the Lake Tahoe Basin (Dingler et al., 2009). In Lake Iznik, these sedimentary geometries can be explained by significant tectonic displacement along the MNAF, which formed the southern border of the lake (**Fig. 1b**).

5.1 Contourites in Lake Iznik

Contourites are sediments deposited or significantly reworked by bottom currents, mainly thermohaline- and wind-driven currents, and are highly variable in both time and space (Rebesco, 2018). Seismic Sequences IV, III, and II exhibit the characteristics of typical contourite drifts, which accumulated between ~45 and ~10 ka cal. BP. The onset of this drift-dominated sedimentation pattern occurred after the deposition of seismic Sequence V (orange HAR), which still features a draping geometry (**Fig. 2**). The lateral thickness variations in the overlying drift sequences had a significant impact on the palaeobathymetry of the lake, which became superimposed with the impact of active faults (e.g. Öztürk et al., 2009; Gastineau et al., 2021). Öztürk et al. (2009) previously interpreted this sediment shape as syndepositional folding associated with active faults north and south of the ridge. However, this explanation of folding is difficult to support in this extensional geological context.

Contourite systems have been observed in large deep lakes, such as Lake Superior (Johnson et al., 1980), Lake Malawi (Rosendahl and Livingstone, 1983), Lake Baikal (Ceramicola et al., 2001), Lake Geneva (Girardclos et al., 2003), Lago Cardiel (Gilli et al., 2005), and Lake Prespa (Wagner et al., 2012). These studies interpreted seismic sequence geometries, similar to those found in Lake Iznik, as drift deposits induced by lake currents, which were caused by strong winds. All of the previous studies postulated that a current pattern characterised by a circular gyre leads to i) higher sedimentation rates in central areas of the lake where current velocities are low, and ii) moat structures at the edges of the basin where the sedimentation rate is low or even erosion occurs due to the strong currents. Such gyres were already described at the lake surface during the 2010 summer (Viehberg et al., 2012). Therefore, we interpret the onset of drift deposition as starting with Sequence IV because of the enhanced wind stress on the lake surface after ~45 ka cal. BP. The coarser-grained sediments of Unit 'E' of Core IZN21-IV support this interpretation because the finer-

grained sediments may have been removed by the strong current, leaving only the coarser grains in place (**Fig. 7a**). Contourite drift deposition in Lake Iznik terminated at the boundary between Sequences II/I (**Fig. 2**; turquoise HAR at ~10 ka cal. BP), where erosive features are observed 50 m below the current lake level, indicating a potential reorganisation of the current pattern. This change may be attributed to shifts in wind patterns and/or a significant drop in water level before the mentioned time. Furthermore, these results could explain the prolonged duration of the hiatus observed in Core IZN21-IV (**Table 2**).

5.2   Impact of tectonics on the Iznik Basin

Different highstands have been documented in the Iznik Basin, notably at ~20, 60, and 110 m a.l.l. (see section 2.2.1). However, the lake currently drains westwards with an outlet at an elevation of ~85 m a.s.l., making it impossible to record such highstands under present conditions. Nevertheless, two primary hypotheses could explain such observations in the past:

(1) The influence of long-term tectonic processes on palaeoshoreline formation is debated. Some studies minimise the significance of surrounding faults and emphasise the role of past high lake levels in determining palaeoshoreline elevations (e.g. Nümann, 1960; Öztürk et al., 2009). In contrast, we propose that tectonic activity may have impacted relative lake-level changes, notably due to the subsidence of the Iznik Basin caused by its right-lateral transtensional structure. This subsidence implies that the exposed palaeoshorelines were once higher than their current elevation, which presents a challenge to explain. In contrast, Yaltırak et al., (2012) reported a mean tectonic uplift rate of 0.3 ± 0.05 mm yr^{-1} over the past 200 ka for the southern segment of the northern branch of the NAF. This uplift may have also contributed to the creation of these high-elevation palaeoshorelines. Nevertheless, these palaeoshorelines and their topographical characteristics suggest that they formed at some point due to the lake's erosive processes. Consequently, the chronological ages attributed to these palaeoshorelines (denoted "terraces" in Benjelloun et al. 2021) correspond to the period when these sediment surfaces were abandoned due to decreasing lake levels. However, even considering the uplift rate estimated by Yaltırak et al. (2012), the highest palaeoshoreline would have reached an elevation of ~102 m a.s.l. at 27 ka BP if its implication is subtracted from the modern elevation of ~110 m a.s.l. Further research is needed to accomplish two key objectives: (1) accurately determine the extent of local uplift caused by the surrounding faults (specifically, the balance between the normal Gürle and Orhangazi faults in **Fig. 1b**); and (2) assess

19

the rate of the outlet's incision and ascertain whether the observed rise can be adequately explained or whether a hypothetical landslide along the pathway of the current outlet (Karsak Pass; **Fig. 1b**) might be necessary to account for the increased elevation, as it is currently at ~85 m a.s.l.

(2) Ikeda et al. (1991) argued that since the deposition rate of alluvium derived from the precipitous fault scarp on the southern Orhangazi Plain was relatively high, and the narrow outlet of the basin was rapidly buried, causing the lake level to rise. As it occurs today, the outlet and the connection between the Marmara Sea and Lake Iznik have been debated for a decade. Different scenarios have been proposed, postulating the onset of such a westwards draining from the early Khazarian (middle Pleistocene; ca. 300 ka BP) to the Holocene (Aktaş et al., 2021; Doğan et al., 2015; İslamoğlu, 2009; Nazik et al., 2011). For example, Meriç et al., (2018) and Sagular et al., (2018) indicated that Lake Iznik experienced a marine depositional environment characterised by "littoral, estuary, or lagoon environments from late Pleistocene to the Holocene." based on flora and fauna assemblages found in sediment cores. It is therefore thought that the hydrological separation of the Gulf of Gemlik is due to the activity of the fault. Yaltırak et al. (2012) suggested contrasting potential connections between 380-420 and 475-575 ka ago but excluded connection possibilities during the late Pleistocene–Holocene because of the abovementioned uplift rate. Based on the recorded elevated water levels in the late Pleistocene, we contend that Lake Iznik was not a bay within the Marmara Basin during this period; instead, it functioned as an independent lacustrine basin since at least the LGM.

We thus suggest that the lake-level variations identified through our data do not stem solely from tectonic movements. Although tectonic activity in this region could contribute to an overall directional trend in lake levels and explain why high stands are recorded, tectonic activity alone cannot explain the recurrent cycles of highstands/lowstands, which have relatively rapid and high variations. These cyclic patterns must have arisen due to significant precipitation/evaporation budget variations, such as proposed by Roeser et al., (2016).

5.3   Reconstruction of lake-level fluctuations and implications for palaeohydrology

To reconstruct the lake-level history of Lake Iznik (**Fig. 9a**), we combined our interpretations from seismic and sediment-core data with data from the literature such as pollen, grain size, climate records and other lake-level studies within the Eastern Mediterranean region. Roeser et al. (2016) used different proxies to study the

20

relative lake-level fluctuations. For example, they related increased aragonite precipitation to a low lake level for the Holocene epoch, as explained earlier. In addition, the coarse silt/clay ratio has also been used as a lake-level proxy, upon ensuring the absence of event deposits, such as turbidites, in the sedimentary sequence, as their presence could lead to misinterpretations (Roeser et al., 2016; **Fig. 9b**). Finer sediments are deposited during periods of the deeper water column (suspended fine silt and medium-to-coarse silt), while coarser sediments are interpreted to be deposited when lake level is lower (and hence the shoreline closer to the coring location).

5.3.1   Late Pleistocene (>45 ka BP) (Sequences V and IV)

The top of Sequence VI (magenta HAR) cannot be accurately dated, but a linear extrapolation of the age model of IZN21-IV estimates an age of ~70 ka BP (**Table 1** and **Fig. 7d**). At this VI/V boundary, the lake level was substantially lower by at least ~60 m, as suggested by the lowest beach ridge and associated lakeward onlap (**Fig. 4a, b**). Furthermore, this lowstand is supported by lakeward-dipping reflections (clinoforms) indicating prograding delta or shorefaces at similar depths in the underlying Sequence VI (**Figs. 2b, d, 4a, b**). The angular unconformity at the top of Sequence VI and its strong and irregular reflection indicate an erosive unconformity likely associated with periods of desiccation during drier climatic conditions (**Fig. 2**). This hypothesis could match the pollen analyses in the Marmara Sea (Biltekin et al., 2023). During Marine Isotope Stage (MIS) 5b, from ~82 to 74 ka BP, the pollen flora in the southern Sea of Marmara indicated relatively cold and dry conditions (Biltekin et al., 2023). Following this lowstand, a transgressional phase with a highstand between ~70 ka BP and ~45 ka cal. BP is documented (Sequence V) based on the observation of the stepwise formation of a series of up to 13 buried palaeoshorelines (beach ridges) at the boundary between Sequences VI/V (**Fig. 2c**; magenta HAR). Additionally, Sequence V exhibits uniform thickness and relatively transparent seismic facies, indicating high lake levels well beyond the modern shoreline (Gilli et al., 2005); **Fig. 2**). This finding is also consistent with pollen records in the Marmara Sea, where a relatively cool climate and significant rainfall were described during MIS-4 (from 70 to 50.2 ka cal. BP) (Biltekin et al., 2023).

5.3.2   Pre-LGM (45 ka cal. BP – 22 ka cal. BP) (Sequences IV and III)

From at least the end of MIS-3 (~31 ka cal. BP) to ca. 24 ka cal. BP, we propose a high lake level based on i) the data from Roeser (2014), who suggested a high lake level based on a consistent, very fine clayey matrix

21

(**Fig. 9b**), ii) the palaeoshoreline S1 dated to $27.0^{+10.9}_{-13.0}$ ka BP indicating a highstand at ~110 m a.l.l at that time and iii) a cool climate with some humidity described from pollen in the Marmara Sea for the second part of MIS-3 (45–30 ka cal. BP) and the earliest MIS-2 (30–27.5 ka cal. BP) (Biltekin et al., 2023).

In addition, Lake Van in Eastern Anatolia, Turkey, shows evidence of a subsequent and coincident transgressional and high lake-level phase between 48 and 29 ka cal. BP (Kuzucuoğlu et al., 2010). Furthermore, the high palaeoshoreline, occurring at approximately 26–24.5 ka cal. BP, resembles the terrace in Lake Van, coincidentally reaching 110 m above its present lake level (Cukur et al., 2014). This suggests that both lake levels remained relatively high for an extended period. A lake-level highstand also occurred between 27.2 and 24.6 ka cal. BP in the Konya Basin in south-central Turkey, reflecting consistent climate patterns (Roberts et al., 1999). Collectively, this evidence indicates that the highest lake levels in the eastern Mediterranean region were reached between 27 and 24 ka cal. BP (e.g. Tzedakis, 2007). However, Lake Hazar in Eastern Anatolia, Turkey, presented a lowstand during the MIS-2 (29-23 ka cal. BP) (Eriş et al., 2019). This could be explained by differences in latitude, which significantly affects the precipitation/evaporation balance in Anatolian lakes.

Although it appears to be a climate-driven phenomenon, the high lake level in Lake Iznik during this period contradicts the fact that the Sea of Marmara was also a lake at the same time. This discrepancy arises from the interruption of the water connection between the Mediterranean and Marmara seas due to a global decrease in sea level (Filikci et al., 2017; Leroy et al., 2023; **Fig. 9e**). In the open system of Lake Iznik, this divergence suggested that an obstruction, such as a landslide in the Karsak Pass, may have blocked or at least diminished the water flow causing the water level in Lake Iznik to rise. Further research should explore this aspect in more detail.

5.3.3 The LGM (20 +/- 2 ka cal. BP) (light-green HAR)

In the region of Uludağ Mountain in NW Turkey (ca. 45 km SW of Lake Iznik), the LGM has been dated to 20.3 +/- 1.5 ka BP (Zahno et al., 2010) using surface exposure dating applied to glacially transported boulders, ice-moulded bedrock, and unaffected bedrock outcrops. This age corresponds to the time of the deposition at the base of Sequence II. We previously showed that from the onset of Sequence IV to the end of Sequence II, sedimentation in Lake Iznik was predominantly influenced by contourite drifts, posing challenges in interpreting seismic geometries and lithologies in Core IZN21-IV in terms of palaeolake levels. Nonetheless, north of this area, the base of Sequence II (light green HAR – 22 ka cal. BP) exhibits an erosive

discordance ~20 m below the modern lake level, truncating Sequences III, V, and VI. This observation suggests a rapid decrease in lake level during the LGM, consistent with (1) the palaeoshoreline S2 at ~60 m a.l.l., which has an abandonment age of $19.6^{+7.7}_{-7.2}$ ka BP, and then (2) the beach rocks dated at 20.285 ± 2.067 ka (Erginal et al., 2012), suggesting that during this period, the lake maintained a level similar to that of today (ca. 85 m a.s.l.). Additional tectonic data would allow us to quantify the impact of tectonics on the altitude of this palaeoshoreline. The analysis of pollen assemblages from the Lake Iznik watershed during the LGM also revealed minimal vegetation productivity, implying low precipitation (Miebach et al., 2016), which was supported by the lower sedimentation rate during this period. Collectively, these observations point to a decrease in lake level during the LGM. Furthermore, Öztürk et al. (2009) interpret fossil lake terraces north and south of Lake Iznik as indicators of past low lake levels during the LGM, although dating of these terraces was lacking.

On the other hand, interpretations of the composite core IZN09/LC2&LC3 vary. Initially, lithic pebbles and shell fragments were interpreted as indicative of a high-energy environment, suggesting a low lake level during the LGM (Roeser et al., 2012). Subsequent data, particularly grain-size data, later support the presence of a deep-water pelagic system—potentially ice-covered—during the LGM. A lake-level drop is proposed to have occurred only after the LGM, around ~18 ka cal. BP (**Fig. 9b, c**; Roeser et al., 2016). In this scenario, the lithic fragments would be considered as dropstones or till. Yet, the presence of *Dreissena* sp. fragments of a fining-upwards size during the LGM challenges the hypothesis of a deep-water column, as these fragments generally need energy to be fragmented, and their size, which tend to be finer toward the top, could indicate that the sediments have been reworked. Despite differing interpretations, our findings align with those of Roeser et al. (2016) in demonstrating a decrease in lake level during the LGM. It is important to note that even if the lake level decreased, the water column remained deep enough to explain the presence of very fine clay matrix sediments in the core IZN09/LC2&LC3 location. In the Gulf of Gemlik (formerly Gemlik Lake, **Fig. 9e**), a seismic and bathymetric investigation indicated signs of lowstand predating 18 ka cal. BP, implying a dry regional climate during the LGM (Eriş et al., 2019).

After 24 ka cal. BP, there was a predominant trend of decreasing lake levels in the Mediterranean region (Tzedakis, 2007), as in central Anatolia, the Konya LGM mega-lake disappeared ca. 20.5 ka cal. BP (Fontugne et al., 1999). However, some lakes exhibit contrasting patterns: for example, in eastern Turkey, Lake Van experienced a highstand >70 m above its present level during the LGM, and a decrease in lake

level was observed only from ca. 20 to 15 ka cal. BP (**Fig. 9d**) (Landmann et al., 1996; Stockhecke et al., 2014; **Fig. 9d**). Similarly, Lake Tuz, which is situated in Central Anatolia, experienced a lake level that was more than 15 m higher than the current level at 20 – 17 ka cal. BP (Kashima, 2002). This trend was mirrored by Lake Lisan (Dead Sea Basin), which also exhibited high lake levels during the LGM (Bartov et al., 2002). These observations, however, do not contradict the low lake level in Lake Iznik. Instead, they are attributed to the antiphase relationship between Eastern Anatolia and the Levant, which diverged from the North Atlantic-controlled climate during the LGM (Kushnir and Stein, 2010; Tzedakis, 2007).

5.3.4   Post-LGM to early Holocene (18 ka cal. BP - 10 ka cal. BP) (Sequence II)

During the deglaciation, the lake level was likely still low. In the sediment core IZN09/LC2&LC3, the abrupt emergence of aragonite at approximately 18 ka cal. BP (**Fig. 9**) aligns with the decrease in the ln(Mn/Fe) ratio from the light-green to turquoise HARs in Core IZN21-IV (**Fig. 7**). This shift suggested a geochemical response to rapid water column mixing over shorter intervals (Roeser, 2014). Both findings correspond with the decrease in lake level from ~22 to 16.5 ka cal. BP, followed by a subsequent increase in lake level from ~16.5 to 14.7 cal. BP (Roeser, 2014).

This rising trend was then followed by a drop in lake level as shown by a sudden increase in aragonite content and by the relatively coarser grain sizes (**Fig. 9c**, Roeser, 2014). This coincides with the beach rocks dated to 15 and 9 ka BP suggesting a rise in lake level (Öztürk et al., 2016). In Lake Van, a drastic lake-level lowstand at ca. 18 ka BP (Landmann et al., 1996; Stockhecke et al., 2014), also documented in the Konya Basin (Roberts, 1983), was followed by a lake-level increase at ca. 15 ka cal. BP, illustrating this period of rapid and brief changes (**Fig. 9d**). This observation aligns with our findings, suggesting that Lake Iznik did not experience a drastic drop, as no erosive features are observed in the seismic data. Instead, it points to a decreasing water column, similar to the observations in Lake Lisan from ~25 to 10 ka cal. BP (Torfstein et al., 2013).

5.3.5   Early Holocene to the present (<10 ka cal. BP) (Sequence I)

The onset of Sequence I (turquoise HAR) at ~10 ka cal. BP exhibited erosive characteristics spanning the entire basin. This sequence corresponds to a time when the lake level was significantly lower, ~50 m below the current level (**Fig. 10**). A few examples are shown in **Fig. 10**. First, two erosive unconformities between the turquoise HAR and the underlying seismic sequence are observed at ~66 and ~73 ms (~50 and ~55 m

below the modern lake level) (**Fig. 10a, b**). Other features can also illustrate a palaeolowstand, such as the palaeodelta at a depth of ~73 ms (~55 m) in the southwestern part of the lake, likely a palaeodelta of the Kocadere River (**Fig. 10c**). A palaeoshoreline (beach ridge) in the eastern part of the lake at ~65 ms (~49 m) (**Fig. 10d**) shows that the lake was at that level for at least a few decades.

The lowstand seems to align with the period ranging from approximately 14 to 9 ka cal. BP that has been documented in a previous study as being associated with an increase in the aragonite content in the sediment, which is also in agreement with the TOC/N and grain-size data from sediment core IZN09/LC2&LC3 (**Fig. 9c**; Roeser et al., 2016). Moreover, this interval corresponds closely to the hiatus observed in three long sediment cores (IZN21-I, IZN21-II, and IZN21-III) extracted from the Iznik Fault location (Duarte et al., 2023). The hiatus spans from ca. 10.2 to ca. 8.6 ka cal. BP at similar water depths (**Fig. 9a**). Additionally, core IZN19_12 exhibited fine-grained lacustrine sedimentation at 6.5 ka cal. BP, consistent with an increasing lake level prior to that age (**Figs. 6, 9**). The Mediterranean and Black Sea reconnection, dated precisely at 9 ka cal. BP (e.g., Soulet et al., 2011), may have led to increased moisture in the climate system, as hypothesised by Roeser (2014), possibly contributing to a rise in the level of Lake Iznik. This also supports our interpretation of changes in internal lake currents (see section 5.1). Between ~14 and 9 ka cal BP, the Lake Iznik basin was likely unattractive for habitation due to low lake levels, relatively more saline water, and steep marginal lake slopes (Roeser, 2014). After 9 ka cal. BP, the lake level increased, and beachrocks formed between 7.9 and 5.6 ka BP, indicating that the lake level elevation was similar to that recorded today (**Fig. 9a;** Öztürk et al., 2016). Indeed, Lake Iznik seems to have reached its modern level at 6.5 ka cal. BP (Roeser, 2014; Öztürk et al., 2016; Benjelloun et al., 2021; **Fig. 9**). In particular, the initial settlements in the Iznik Basin emerged shortly after the lake's water level began to rise in the Middle Holocene. There is no evidence of a significant decrease in lake level following the last one highlighted by the turquoise HAR. However, several markers demonstrate ongoing fluctuations in the lake's water level, as documented by a previous palaeoenvironmental study (Ülgen et al., 2012) and the submerged Basilica discovered in 2014 at a depth of two metres (Şahin, 2014). This basilica implies that the lake level was lowered by at least two metres during its construction, followed by an increase that submerged it. In 2023, this basilica was almost entirely visible above the waterline (**Fig. 1c**). However, discerning between human causes and climatic impacts in the recent time frames is challenging.

6   SUMMARY AND CONCLUSIONS

In conclusion, our comprehensive analysis of the palaeohydrological history of Lake Iznik provides valuable insights into the complex interplay of climatic, tectonic, and environmental factors that shaped the evolution of this lake basin and contribute to our understanding of the region's geological and environmental dynamics. The following key findings and their broader implications emerge:

(1) **Identification of contourite drifts.** The recognition of contourite drifts in the lake sediment points to past strong currents, shedding light on the dynamic nature of the lake's depositional patterns between ~45 and ~10 ka cal. BP. This insight, reflecting increased wind-stress on the lake surface during that time, has broader implications for understanding regional wind conditions during this timeframe.

(2) **Tectonic processes and basin evolution.** This study underscores the influence of tectonic processes, particularly the right-lateral transtensional structure of the Iznik Basin, which emerges as an important driver of the palaeoshoreline's location. The discussion of subsidence, uplift rates and fault activity enriches our understanding of the geological context of the basin while highlighting the need for further research. Tectonic activity certainly impacted the subsidence of the basin and the uplift of its northern margin, which requires further quantification. In addition, seismic activity may have affected the lake's unique and narrow outlet and potential inlets.

(3) **Lake-level fluctuations and climate sensitivity.** The reconstruction of lake-level fluctuations from the late Pleistocene to the present day has revealed distinct phases of high- and lowstands. Remarkable periods, such as the LGM and the early Holocene, demonstrate the sensitivity of Lake Iznik to regional and global climate change. For example, from ca. 14 to ca. 10 ka cal. BP, a major lowstand ~50 m below the present-day lake level, indicates a drier climate. Since then, the rapid increase in lake level matches the reconnection event with the Mediterranean and Black Seas, likely due to increased moisture in the climate system, further underlining the dynamic nature of this lake system.

(4) **Archaeological evidence and human-environment interactions**. The archaeological evidence, including submerged structures such as the basilica and the fact that the initial settlements in the Iznik Basin emerged shortly after the lake's water level began to rise in the middle Holocene, provides a convincing link between environmental change and human settlement, highlighting the

interconnectedness of natural processes and societal developments.

In conclusion, our results and data review contribute to a better understanding of palaeoenvironments and climate dynamics in the western Mediterranean region during the last 70 ka.

Data availability and resources

The IZN19_12 and IZN21-IV core locations and sampling procedures can be found in the French National Cyber-core repository (https://cybercarotheque.fr/index.php). All the raw data can be provided by the authors upon request.

Author contributions

RG, FA, SF, PS, PR, SG, MS, WR, AG, SF, FN, and JdS participated in at least one fieldwork (seismic acquisition, sediment core sampling). RG, FA, and SF interpreted the seismic data. RG and PS performed the interpretation and data acquisition in the sediment cores IZN19_12 and IZN21-IV. ED did the tephra

27

analysis of IZN21-IV. PR performed the interpretation and data acquisition on the IZN09 sediment cores. RG wrote the manuscript draft; All the authors reviewed and edited the manuscript. PS and JdS supervised RG during his PhD thesis. JdS is the PI of the ANR Project leading to this manuscript.

References

Abbott, M.B., Anderson, L., 2009. Lake-Level Fluctuations, in: Gornitz, V. (Ed.), Encyclopedia of Paleoclimatology and Ancient Environments. Springer Netherlands, Dordrecht, pp. 489–492. https://doi.org/10.1007/978-1-4020-4411-3_121

Aktaş, G., Hisarli, Z.M., Demirel, A.S., 2021. High-resolution total field magnetic anomaly maps of Lake İznik (NW Turkey): assessment of faults which play important roles in tectonics of the lake. Mar Geophys Res 42, 20. https://doi.org/10.1007/s11001-021-09442-0

Anselmetti, F.S., Ariztegui, D., De Batist, M., Catalina Gebhardt, A., Haberzettl, T., Niessen, F., Ohlendorf, C., Zolitschka, B., 2009. Environmental history of southern Patagonia unravelled by the seismic stratigraphy of Laguna Potrok Aike. Sedimentology 56, 873–892. https://doi.org/10.1111/j.1365-3091.2008.01002.x

Ariztegui, D., Gilli, A., Anselmetti, F.S., Goñi, R.A., Belardi, J.B., Espinosa, S., 2010. Lake-level changes in central Patagonia (Argentina): crossing environmental thresholds for Lateglacial and Holocene human occupation. Journal of Quaternary Science 25, 1092–1099. https://doi.org/10.1002/jqs.1352

Bartov, Y., Stein, M., Enzel, Y., Agnon, A., Reches, Z., 2002. Lake Levels and Sequence Stratigraphy of Lake Lisan, the Late Pleistocene Precursor of the Dead Sea. Quat. res. 57, 9–21. https://doi.org/10.1006/qres.2001.2284

Bashah, S., Eberli, G.P., Anselmetti, F.S., 2024. Archive for the East Australian Current: carbonate contourite depositional system on the Marion Plateau, Northeast Australia. Marine Geology 469, 107224.

Benjelloun, Y., 2017. The middle strand of the North Anatolian fault in Iznik region : insights from geomorphology and archeoseismology (Doctoral dissertation). Université Grenoble Alpes.

Benjelloun, Y., de Sigoyer, J., Garambois, S., Carcaillet, J., Klinger, Y., 2021. Segmentation and Holocene Behavior of the Middle Strand of the North Anatolian Fault (NW Turkey). Tectonics 40, e2021TC006870. https://doi.org/10.1029/2021TC006870

Berger, A., Loutre, M.-F., Kaspar, F., Lorenz, S., 2007. 2. Insolation during interglacial, in: Developments in Quaternary Sciences. Elsevier, pp. 13–27.

Biltekin, D., Eriş, K.K., Çağatay, M.N., Henry, P., Yakupoğlu, N., 2023. New records of vegetation and climate changes in the Sea of Marmara during the Marine Isotope Stages 3, 4 and 5 (ac). Quaternary International 667, 1–18.

Blaauw, M., Christen, J.A., 2011. Flexible paleoclimate age-depth models using an autoregressive gamma

process. Bayesian Analysis 6, 457–474. https://doi.org/10.1214/11-BA618

Çağatay, M.N., Wulf, S., Sancar, Ü., Özmaral, A., Vidal, L., Henry, P., Appelt, O., Gasperini, L., 2015. The tephra record from the Sea of Marmara for the last ca. 70 ka and its palaeoceanographic implications. Marine Geology 361, 96–110. https://doi.org/10.1016/j.margeo.2015.01.005

Ceramicola, S., Rebesco, M., De Batist, M., Khlystov, O., 2001. Seismic evidence of small-scale lacustrine drifts in Lake Baikal (Russia). Marine Geophysical Researches 22, 445–464. https://doi.org/10.1023/A:1016351700435

Cukur, D., Krastel, S., Schmincke, H.U., Sumita, M., Tomonaga, Y., Namık Çağatay, M., 2014. Water level changes in Lake Van, Turkey, during the past ca. 600 ka: climatic, volcanic and tectonic controls. Journal of paleolimnology 52, 201–214. https://doi.org/10.1007/s10933-014-9788-0

Cukur, D., Krastel, S., Tomonaga, Y., Schmincke, H.-U., Sumita, M., Meydan, A.F., Çağatay, M.N., Toker, M., Kim, S.-P., Kong, G.-S., Horozal, S., 2017. Structural characteristics of the Lake Van Basin, eastern Turkey, from high-resolution seismic reflection profiles and multibeam echosounder data: geologic and tectonic implications. Int J Earth Sci (Geol Rundsch) 106, 239–253. https://doi.org/10.1007/s00531-016-1312-5

Davies, S.J., Lamb, H.F., Roberts, S.J., 2015. Micro-XRF core scanning in palaeolimnology: recent developments. Micro-XRF studies of sediment cores: Applications of a non-destructive tool for the environmental sciences 189–226.

Davraz, A., Sener, E., Sener, S., 2019. Evaluation of climate and human effects on the hydrology and water quality of Burdur Lake, Turkey. Journal of African Earth Sciences 158, 103569. https://doi.org/10.1016/j.jafrearsci.2019.103569

De Vivo, B., Rolandi, G., Gans, P.B., Calvert, A., Bohrson, W.A., Spera, F.J., Belkin, H.E., 2001. New constraints on the pyroclastic eruptive history of the Campanian volcanic Plain (Italy). Mineralogy and Petrology 73, 47–65. https://doi.org/10.1007/s007100170010

Dingler, J., Kent, G., Driscoll, N., Babcock, J., Harding, A., Seitz, G., Karlin, B., Goldman, C., 2009. A high-resolution seismic CHIRP investigation of active normal faulting across Lake Tahoe Basin, California-Nevada. GSA Bulletin 121, 1089–1107. https://doi.org/10.1130/B26244.1

Doğan, B., Tüysüz, O., Şanlı, F.B., 2015. Tectonostratigraphic evolution of the basins on the southern branch of the North Anatolian Fault System in the SE Marmara Region, Turkey. Int J Earth Sci (Geol Rundsch) 104,

389–418. https://doi.org/10.1007/s00531-014-1083-9

Duarte, E., Sabatier, P., De Sigoyer, J., Gastineau, R., Anselmetti, F.S., Rapuc, W., Fabbri, S.C., Domenge, J., Şahin, M., Gündüz, S., Gebhardt, A.C., Niessen, F., Franz, S., 2023. Long-term lacustrine paleoseismicity along the Middle Strand of the North Anatolian Fault (MNAF), NW Turkey, in: Abstract No.1240655. Presented at the AGU23 Meeting, San Francisco, California, USA.

Erginal, A.E., Erenoğlu, R.C., Yıldırım, C., Selim, H.H., Kıyak, N.G., Erenoğlu, O., Ulugergerli, E., Karabıyıkoğlu, M., 2021. Co-seismic beachrock deformation of 8th century AD Earthquake in Middle Strand of North Anatolian Fault, Lake Iznik, NW Turkey. Tectonophysics 799, 228690. https://doi.org/10.1016/j.tecto.2020.228690

Erginal, A.E., Kıyak, N.G., Öztürk, M.Z., Avcıoğlu, M., Bozcu, M., Yiğitbaş, E., 2012. Cementation characteristics and age of beachrocks in a fresh-water environment, Lake İznik, NW Turkey. Sedimentary Geology 243–244, 148–154. https://doi.org/10.1016/j.sedgeo.2011.10.012

Eriş, K.K., Sabuncu, A., Gasperini, L., Polonia, A., Kındap, T., 2019. Influence of climate on the late Pleistocene depositional history of the Gulf of Gemlik (Sea of Marmara). Geo-Marine Letters 39, 205–221. https://doi.org/10.1007/s00367-019-00568-0

Fenn, K., Thomas, D.S., Durcan, J.A., Millar, I.L., Veres, D., Piermattei, A., Lane, C.S., 2021. A tale of two signals: Global and local influences on the Late Pleistocene loess sequences in Bulgarian Lower Danube. Quaternary Science Reviews 274, 107264. https://doi.org/10.1016/j.quascirev.2021.107264

Filikci, B., Eriş, K.K., Çağatay, N., Sabuncu, A., Polonia, A., 2017. Late glacial to Holocene water level and climate changes in the Gulf of Gemlik, Sea of Marmara: evidence from multi-proxy data. Geo-Marine Letters 37, 501–513. https://doi.org/10.1007/s00367-017-0498-2

Fontugne, M., Kuzucuoğlu, C., Karabiyikoğlu, M., Hatte, C., Pastre, J.-F., 1999. From Pleniglacial to Holocene: a 14C chronostratigraphy of environmental changes in the Konya Plain, Turkey. Quaternary science reviews 18, 573–591.

Fouinat, L., Sabatier, P., David, F., Montet, X., Schoeneich, P., Chaumillon, E., Poulenard, J., Arnaud, F., 2018. Wet avalanches: long-term evolution in the Western Alps under climate and human forcing. Climate of the Past 14, 1299–1313. https://doi.org/10.5194/cp-14-1299-2018

Gastineau, R., De Sigoyer, J., Sabatier, P., Fabbri, S.C., Anselmetti, F.S., Develle, A.L., Şahin, M., Gündüz, S., Niessen, F., Gebhardt, A.C., 2021. Active Subaquatic Fault Segments in Lake Iznik Along the Middle

Strand of the North Anatolian Fault, NW Turkey. Tectonics 40, e2020TC006404. https://doi.org/10.1029/2020tc006404

Gastineau, R., Sabatier, P., Fabbri, S.C., Anselmetti, F., Roeser, P., Findling, N., Şahin, M., Gündüz, S., Arnaud, F., Franz, S., others, 2023. Lateral variations in the signature of earthquake-generated deposits in Lake Iznik, NW Turkey. The Depositional Record. https://doi.org/10.1002/dep2.232

Geyer, B., Dalongeville, R., Lefort, J., 2001. Les niveaux du lac de Nicée au Moyen-Âge, in: Castrum 7: Zones côtières littorales dans le monde Méditerranéen au Moyen Âge : défense, peuplement, mise en valeur, Ecole française de Rome. Casa de Velázquez (in French).

Gilli, A., Anselmetti, F.S., Ariztegui, D., Beres, M., McKenzie, J.A., Markgraf, V., 2005. Seismic stratigraphy, buried beach ridges and contourite drifts: the Late Quaternary history of the closed Lago Cardiel basin, Argentina (49°S): Seismic stratigraphy of Lago Cardiel, Argentina. Sedimentology 52, 1–23. https://doi.org/10.1111/j.1365-3091.2004.00677.x

Girardclos, S., Baster, I., Wildi, W., Pugin, A., Rachoud-Schneider, A.-M., 2003. Bottom-current and wind-pattern changes as indicated by Late Glacial and Holocene sediments from western Lake Geneva (Switzerland), in: Lake Systems from the Ice Age to Industrial Time. Springer, pp. 39–48.

Guédron, S., Delaere, C., Fritz, S.C., Tolu, J., Sabatier, P., Devel, A.-L., Heredia, C., Vérin, C., Alves, E.Q., Baker, P.A., 2023. Holocene variations in Lake Titicaca water level and their implications for sociopolitical developments in the central Andes. Proceedings of the National Academy of Sciences 120, e2215882120. https://doi.org/10.1073/pnas.2215882120

Ikeda, Y., Herece, E., Svgai, T., Isikara, A.M., 1991. Post glacial crustal deformation associated with slip on the Western part of the North Anatolian Fault Zone in the Iznik Lake Basin, Turkey. Bulletin of the Department of Geography University of Tokyo 23, 13–23.

İslamoğlu, Y., 2009. Middle Pleistocene bivalves of the İznik lake basin (Eastern Marmara, NW Turkey) and a new paleobiogeographical approach. Int J Earth Sci (Geol Rundsch) 98, 1981–1990. https://doi.org/10.1007/s00531-008-0344-x

Jenny, J.-P., Anneville, O., Arnaud, F., Baulaz, Y., Bouffard, D., Domaizon, I., Bocaniov, S.A., Chèvre, N., Dittrich, M., Dorioz, J.-M., others, 2020. Scientists' warning to humanity: rapid degradation of the world's large lakes. Journal of Great Lakes Research 46, 686–702. https://doi.org/10.1016/j.jglr.2020.05.006

Jochum, K.P., Dingwell, D.B., Rocholl, A., Stoll, B., Hofmann, A.W., Becker, S., Besmehn, A., Bessette,

D., Dietze, H.-J., Dulski, P., others, 2000. The preparation and preliminary characterisation of eight geological MPI-DING reference glasses for in-situ microanalysis. Geostandards Newsletter 24, 87–133. https://doi.org/10.1111/j.1751-908X.2000.tb00590.x

Jochum, K.P., Nohl, U., Herwig, K., Lammel, E., Stoll, B., Hofmann, A.W., 2005. GeoReM: a new geochemical database for reference materials and isotopic standards. Geostandards and Geoanalytical Research 29, 333–338.

Jochum, K.P., Stoll, B., Herwig, K., Willbold, M., Hofmann, A.W., Amini, M., Aarburg, S., Abouchami, W., Hellebrand, E., Mocek, B., Raczek, I., Stracke, A., Alard, O., Bouman, C., Becker, S., Dücking, M., Brätz, H., Klemd, R., Bruin, D. de, Canil, D., Cornell, D., Hoog, C.-J. de, Dalpé, C., Danyushevsky, L., Eisenhauer, A., Gao, Y., Snow, J.E., Groschopf, N., Günther, D., Latkoczy, C., Guillong, M., Hauri, E.H., Höfer, H.E., Lahaye, Y., Horz, K., Jacob, D.E., Kasemann, S.A., Kent, A.J.R., Ludwig, T., Zack, T., Mason, P.R.D., Meixner, A., Rosner, M., Misawa, K., Nash, B.P., Pfänder, J., Premo, W.R., Sun, W.D., Tiepolo, M., Vannucci, R., Vennemann, T., Wayne, D., Woodhead, J.D., 2006. MPI-DING reference glasses for in situ microanalysis: New reference values for element concentrations and isotope ratios. Geochemistry, Geophysics, Geosystems 7. https://doi.org/10.1029/2005GC001060

Johnson, Carlson, T.W., Evans, J.E., 1980. Contourites in Lake Superior. Geol 8, 437. https://doi.org/10.1130/0091-7613(1980)8<437:CILS>2.0.CO;2

Kashima, K., 2002. Environmental and climatic changes during the last 20,000 years at Lake Tuz, central Turkey. CATENA 48, 3–20. https://doi.org/10.1016/S0341-8162(02)00006-1

Köppen, W., 1900. Versuch einer Klassifikation der Klimate, vorzugsweise nach ihren Beziehungen zur Pflanzenwelt. Geographische Zeitschrift 6, 593–611.

Kushnir, Y., Stein, M., 2010. North Atlantic influence on 19th–20th century rainfall in the Dead Sea watershed, teleconnections with the Sahel, and implication for Holocene climate fluctuations. Quaternary Science Reviews 29, 3843–3860. https://doi.org/10.1016/j.quascirev.2010.09.004

Kuzucuoğlu, C., Christol, A., Mouralis, D., Doğu, A.-F., Akköprü, E., Fort, M., Brunstein, D., Zorer, H., Fontugne, M., Karabiyikoğlu, M., Scaillet, S., Reyss, J.-L., Guillou, H., 2010. Formation of the Upper Pleistocene terraces of Lake Van (Turkey). Journal of Quaternary Science 25, 1124–1137. https://doi.org/10.1002/jqs.1431

Landmann, G., Reimer, A., Kempe, S., 1996. Climatically induced lake level changes at Lake Van, Turkey,

during the Pleistocene/Holocene transition. Global Biogeochemical Cycles 10, 797–808. https://doi.org/10.1029/96GB02347

Le Maitre, R., Bateman, P., Dudek, A., Keller, J., 1989. Lameyre Le Bas MJ, Sabine PA, Schmid R, Sorensen H, Streckeisen A, Woolley AR, Zanettin B (1989) A classification of igneous rocks and glossary of terms. Blackwell, Oxford.

Lê, S., Josse, J., Husson, F., 2008. FactoMineR: An R Package for Multivariate Analysis. J. Stat. Soft. 25. https://doi.org/10.18637/jss.v025.i01

Lefebvre, P., Sabatier, P., Mangeret, A., Gourgiotis, A., Le Pape, P., Develle, A.-L., Louvat, P., Diez, O., Reyss, J.-L., Gaillardet, J., others, 2021. Climate-driven fluxes of organic-bound uranium to an alpine lake over the Holocene. Science of the Total Environment 783, 146878. https://doi.org/10.1016/j.scitotenv.2021.146878

Leroy, S.A.G., Henry, P., Marret, F., Pailles, C., Licari, L., Kende, J., Rostek, F., Bard, E., 2023. Dinocyst assemblages and water surface conditions in the Sea of Marmara during MIS 6 and 5 from two long cores. Quaternary Science Reviews 314, 108229. https://doi.org/10.1016/j.quascirev.2023.108229

Lezzar, K.E., Tier, J.-J., 2002. Control of normal fault interaction on the distribution of major Neogene sedimentary depocenters, Lake Tanganyika, East African rift. Bulletin 86. https://doi.org/10.1306/61EEDC1A-173E-11D7-8645000102C1865D

Lichter, J., 1995. Lake Michigan beach-ridge and dune development, lake level, and variability in regional water balance. Quaternary Research 44, 181–189. https://doi.org/10.1006/qres.1995.1062

Meriç, E., Nazik, A., Yümün, Z.Ü., Büyükmeriç, Y., Avşar, N., Yildiz, A., Sagular, E.K., Koral, H., Gökaşan, E., 2018. Fauna and flora of drilling and core data from the İznik Lake: The Marmara and the Black Sea connection. Quaternary International 486, 156–184. https://doi.org/10.1016/j.quaint.2017.08.067

Metrich, N., Rutherford, M., 1992. Experimental study of chlorine behavior in hydrous silicic melts. Geochimica et Cosmochimica Acta 56, 607–616. https://doi.org/10.1016/0016-7037(92)90085-W

Miebach, A., Niestrath, P., Roeser, P., Litt, T., 2016. Impacts of climate and humans on the vegetation in northwestern Turkey: palynological insights from Lake Iznik since the Last Glacial. Climate of the Past 12, 575–593. https://doi.org/10.5194/cp-12-575-2016

Nazik, A., Meriç, E., Avşar, N., Ünlü, S., Esenli, V., Gökaşan, E., 2011. Possible waterways between the Marmara Sea and the Black Sea in the late Quaternary: evidence from ostracod and foraminifer assemblages

in lakes İznik and Sapanca, Turkey. Geo-Mar Lett 31, 75–86. https://doi.org/10.1007/s00367-010-0216-9

Nümann, W., 1960. Limnologische Untersuchung einiger anatolischer Seen. Internationale Revue der gesamten Hydrobiologie und Hydrographie 45, 11–54. https://doi.org/10.1002/iroh.19600450103

Özen, A., Ediş, S., Göl, C., 2014. Modelling of minimum water levels of Lake İznik by using time series models.

Öztürk, K., Yaltirak, C., Alpar, B., 2009. The Relationship Between the Tectonic Setting of the Lake İznik Basin and the Middle Strand of the North Anatolian Fault 16.

Öztürk, M., Erginal, A.E., Kiyak, N.G., Demirci, A., Ekinci, Y.L., Curebal, İ., Avcıoglu, M., Ozturk, T., 2016. Records of repeated drought stages during the Holocene, Lake Iznik (Turkey) with reference to beachrock. Quaternary International 408, 16–24. https://doi.org/10.1016/j.quaint.2015.08.077

Özuluğ, M., Altun, Ö., Meriç, N., 2005. On the fish fauna of Lake İznik (Turkey). Turkish Journal of Zoology 29, 371–375.

R Core Team, 2018. R: A Language and Environment for Statistical Computing. R Foundation for Statistical Computing, Vienna, Austria.

Rebesco, M., 2018. Sedimentary Environments: Contourites☆, in: Reference Module in Earth Systems and Environmental Sciences. Elsevier. https://doi.org/10.1016/B978-0-12-409548-9.09094-1

Reimer, P.J., Austin, W.E., Bard, E., Bayliss, A., Blackwell, P.G., Ramsey, C.B., Butzin, M., Cheng, H., Edwards, R.L., Friedrich, M., others, 2020. The IntCal20 Northern Hemisphere radiocarbon age calibration curve (0–55 cal kBP). Radiocarbon 1–33.

Roberts, N., 1983. Age, palaeoenvironments, and climatic significance of late Pleistocene Konya Lake, Turkey. Quaternary research 19, 154–171. https://doi.org/10.1016/0033-5894(83)90002-9

Roberts, N., Black, S., Boyer, P., Eastwood, W.J., Griffiths, H.I., Lamb, H.F., Leng, M.J., Parish, R., Reed, J.M., Twigg, D., Yiğitbaşioğlu, H., 1999. Chronology and stratigraphy of Late Quaternary sediments in the Konya Basin, Turkey: Results from the KOPAL Project. Quaternary Science Reviews 18, 611–630. https://doi.org/10.1016/S0277-3791(98)00100-0

Roeser, P., 2014. Paleolimnology of Lake Iznik (NW Turkey) during the past 31 ka cal BP (Doctoral dissertation). Bonn.

Roeser, P., Franz, S.O., Litt, T., 2016. Aragonite and calcite preservation in sediments from Lake Iznik related to bottom lake oxygenation and water column depth. Sedimentology 63, 2253–2277.

https://doi.org/10.1111/sed.12306

Roeser, P., Franz, S.O., Litt, T., Ülgen, U.B., Hilgers, A., Wulf, S., Wennrich, V., Akçer Ön, S., Viehberg, F.A., Çağatay, M.N., Melles, M., 2012. Lithostratigraphic and geochronological framework for the paleoenvironmental reconstruction of the last ∼36 ka cal BP from a sediment record from Lake Iznik (NW Turkey). Quaternary International 274, 73–87. https://doi.org/10.1016/j.quaint.2012.06.006

Roodenberg, J., 2013. Change in food production and its impact on an early 6th millennium community in northwest Anatolia. The example of Ilıpınar. Praehistorische Zeitschrift 87, 223–235. https://doi.org/10.1515/pz-2012-0015

Rosendahl, B., Livingstone, D., 1983. Rift lakes of East Africa-new seismic data and implications for future research. Episodes Journal of International Geoscience 6, 14–19.

Sabatier, P., Dezileau, L., Briqueu, L., Colin, C., Siani, G., 2010. Clay minerals and geochemistry record from northwest Mediterranean coastal lagoon sequence: Implications for paleostorm reconstruction. Sedimentary Geology 228, 205–217. https://doi.org/10.1016/j.sedgeo.2010.04.012

Sagular, E.K., Yümün, Z.Ü., Meriç, E., 2018. New didemnid ascidian spicule records calibrated to the nannofossil data chronostratigraphically in the Quaternary marine deposits of Lake İznik (NW Turkey) and their paleoenvironmental interpretations. Quaternary International 486, 143–155. https://doi.org/10.1016/j.quaint.2017.08.060

Şahin, M., 2014. İznik Gölü'ndeki Batık Kilise: Deprem Kurbanı Aziz Neophytos. Aktüel Arkeoloji 38 Nisan, 8-10.

Şahin, M., R. Fairchild, M., 2018. Nicea's Underwater Basilica. Biblical Archaeology Review 44:6.

Seeber, L., Sorlien, C., Steckler, M., Cormier, M.-H., 2010. Continental Transform Basins: Why Are They Asymmetric? Eos, Transactions American Geophysical Union 91, 29–30. https://doi.org/10.1029/2010EO040001

Sevink, J., van Bergen, M.J., van der Plicht, J., Feiken, H., Anastasia, C., Huizinga, A., 2011. Robust date for the Bronze Age Avellino eruption (Somma-Vesuvius): 3945 ± 10 calBP (1995 ± 10 calBC). Quaternary Science Reviews 30, 1035–1046. https://doi.org/10.1016/j.quascirev.2011.02.001

Soulet, G., Ménot, G., Lericolais, G., Bard, E., 2011. A revised calendar age for the last reconnection of the Black Sea to the global ocean. Quaternary Science Reviews 30, 1019–1026.

Stockhecke, M., Sturm, M., Brunner, I., Schmincke, H., Sumita, M., Kipfer, R., Cukur, D., Kwiecien, O.,

Anselmetti, F.S., 2014. Sedimentary evolution and environmental history of Lake Van (Turkey) over the past 600 000 years. Sedimentology 61, 1830–1861. https://doi.org/10.1111/sed.12118

Torfstein, A., Goldstein, S.L., Stein, M., Enzel, Y., 2013. Impacts of abrupt climate changes in the Levant from Last Glacial Dead Sea levels. Quaternary Science Reviews 69, 1–7. https://doi.org/10.1016/j.quascirev.2013.02.015

Tzedakis, P., 2007. Seven ambiguities in the Mediterranean palaeoenvironmental narrative. Quaternary Science Reviews 26, 2042–2066. https://doi.org/10.1016/j.quascirev.2007.03.014

Ülgen, U.B., Franz, S.O., Biltekin, D., Çagatay, M.N., Roeser, P.A., Doner, L., Thein, J., 2012. Climatic and environmental evolution of Lake Iznik (NW Turkey) over the last ~4700 years. Quaternary International 274, 88–101. https://doi.org/10.1016/j.quaint.2012.06.016

Viehberg, F.A., Ülgen, U.B., Damcı, E., Franz, S.O., Ön, S.A., Roeser, P.A., Çağatay, M.N., Litt, T., Melles, M., 2012. Seasonal hydrochemical changes and spatial sedimentological variations in Lake Iznik (NW Turkey). Quaternary International 274, 102–111. https://doi.org/10.1016/j.quaint.2012.05.038

Wagner, B., Aufgebauer, A., Vogel, H., Zanchetta, G., Sulpizio, R., Damaschke, M., 2012. Late Pleistocene and Holocene contourite drift in Lake Prespa (Albania/F.Y.R. of Macedonia/Greece). Quaternary International. Editors: Jürgen Richter, Martin Melles, Frank Schäbitz 112–121.

Weltje, G.J., Bloemsma, M., Tjallingii, R., Heslop, D., Röhl, U., Croudace, I.W., 2015. Prediction of geochemical composition from XRF core scanner data: a new multivariate approach including automatic selection of calibration samples and quantification of uncertainties, in: Micro-XRF Studies of Sediment Cores. Springer, pp. 507–534.

Yagbasan, O., Yazicigil, H., Demir, V., 2017. Impacts of climatic variables on water-level variations in two shallow Eastern Mediterranean lakes. Environ Earth Sci 76, 575. https://doi.org/10.1007/s12665-017-6917-x

Yaltırak, C., Ülgen, U.B., Zabcı, C., Franz, S.O., Ön, S.A., Sakınç, M., Çağatay, M.N., Alpar, B., Öztürk, K., Tunoğlu, C., Ünlü, S., 2012. Discussion: a critique of Possible waterways between the Marmara Sea and the Black Sea in the late Quaternary: evidence from ostracod and foraminifer assemblages in lakes İznik and Sapanca, Turkey, Geo-Marine Letters, 2011. Geo-Mar Lett 32, 267–274. https://doi.org/10.1007/s00367-011-0270-y

Zahno, C., Akçar, N., Yavuz, V., Kubik, P.W., Schlüchter, C., 2010. Chronology of Late Pleistocene glacier

variations at the Uludağ Mountain, NW Turkey. Quaternary Science Reviews 29, 1173–1187. https://doi.org/10.1016/j.quascirev.2010.01.012

Figure and Table captions

Figure 1. (a) Map of the study site in the context of global geodynamics. The yellow star denotes the location of Lake Iznik. The abbreviations for the NAF and EAF indicate the North and East Anatolian faults, respectively. (b) Map of the Iznik Basin with a compilation of data used in this study. The digital elevation model (DEM) of the lake catchment (Benjelloun et al., 2021) is complemented by the DEM from the Shuttle Radar Topography Mission (SRTM - 1 arc-second resolution; https://earthexplorer.usgs.gov/). The active faults are represented in red (e.g. Öztürk et al., 2009; Doğan et al., 2015; Benjelloun, 2017; Gastineau et al., 2021). IF refers to the Iznik Fault. The palaeoshorelines S1, S2 and S3 (light grey) are drawn from Benjelloun (2017). The dashed bathymetric contour lines in the lake represent 10-meter intervals (Devlet Su İşleri (DSI); General Directorate of Turkish Hydraulic Works), superimposed on the hillshade bathymetry (2 m grid) from Gastineau et al., (2021), with a sun illumination angle/elevation of 20°N/45° and a vertical exaggeration of 15. The colour scale represents the depth below lake level (b.l.l.), based on a long-term reference lake level of 83.5 m above sea level (a.s.l). The white dots and label names document the locations of the sediment cores presented in this study. WSB, NESB, and SESB refer to the western, northeastern, and southeastern subbasins, respectively. (c) UAV photos of St. Neophytos Basilica in 2018 and 2023 CE, located at the shoreline of the city of Iznik (black arrow).

Figure 2. Two 3.5 kHz seismic sections on the lake's northern shore. Ve denotes "vertical exaggeration". (a) and (c) correspond to the original data. (b) and (d) are the interpreted sections.

Figure 3. Three 3.5 kHz seismic sections (see. **Fig. 1** for location). (a), (c) and (e) correspond to the original data. (c), (d) and (f) are the interpreted sections. Ve denotes "vertical exaggeration". IF refers to the "Iznik Fault". The potential locations of the faults are indicated by dotted lines, while the MNAF is represented by a solid line.

Figure 4. Seismic sections showing beach ridges that formed at the boundary between Sequences VI and V.

Locations are shown in **Fig. 2**. (a, c) Noninterpreted sections. (b, d) Interpreted sections. (b) The lowermost

shoreline shows the minimum depth (below the current lake level) reached during the low lake level. (d)

Other examples of beach ridges illustrating the stepwise transgression following the lowstand.

Figure 5. IZN09/LC2&LC3 composite core: (a) Sedimentary units as described in Roeser et al. (2012); (b)

age model (from Roeser et al., 2016). YD refers to the Younger Dryas and LGM to the Last Glacial

Maximum, characterised by the deposition of the Y2 Santorini tephra. Error bars for age determinations of

the bulk sediments indicate uncertainties related to the reservoir effect (Roeser, 2014). Age determinations

in red are mainly from reworked shells and were not used for calculating the age-depth model (from Roeser

et al., 2016).

Figure 6. IZN19_12 sediment core photos and geochemical data. (a) Photos of the split core before (left) and

after oxidation (right); sedimentary units and facies; ln(Ca/Ti): ln(Mn/Fe); ln(Br/Sr) and ln(Sr/Ca) ratios. (b)

PCA biplot and end-members (variable and individual factor maps). (c) Age model and its respective

sedimentation rate variation curve through time (details in **Table 1**). The location of the sediment core is

shown in **Fig. 3a, b**. Note that this core crosscuts only the turquoise HAR.

Figure 7. IZN21-IV sediment core photos, geochemical data, physical properties, and age model. (a)

Interpreted log of the core, photograph of the split core and sedimentary units, and facies interpretation. (b)

XRF data: ln(Ca/Ti), ln(Mn/Fe), and ln(Sr/Ca) ratios. (c) Density and magnetic susceptibility data. (d) Age

model with three radiocarbon ages that have been rejected for the age model computation due to their

inversion and low amount of carbon (marked in red; details in **Table 1**). The location of the sediment core is

shown in **Fig. 2c**. This core crosscuts the turquoise, light green, dark green and orange HARs, which are

displayed in the figure.

Figure 8. The geochemical composition of tephra samples from the core IZN21-IV. (a) Total alkali-silica

diagram (TAS, (Le Maitre et al., 1989)). Sample IZN21-IV-2T best matches the Cape Riva/Y2 tephra of

Santorini, and sample IZN21-IV-3T best matches the Campanian Ignimbrite/Y5 tephra. (b) Geochemical

biplot FeO vs CaO of tephra sample IZN21-IV-2T (modified from Çağatay et al., 2015). The sample best

matches the Cape Riva/Y2 tephra of Santorini. (c) Geochemical biplot of SiO2 vs. CaO for tephra sample IZN21-IV-3T. (Modified from Çağatay et al., 2015). The sample best matches the Campanian Ignimbrite/Y5 tephra of Vesuvius.

Figure 9. Comparison of (a) a combination of lake-level reconstructions from seismic stratigraphy and literature data; (b) coarse silt-to-clay ratio (black line) of core IZN09/LC2&LC3 with a moving average of window-size ten superimposed (blue line) (from Roeser, 2014). The black arrows indicate changes in lake level. The higher the ratio is, the lower the lake level. (c) Summer insolation values at 40°N originate from (Berger et al., 2007) and aragonite concentrations originate from Roeser et al., 2016. The scales are upside down, so the curves can be easily compared with lake-level fluctuations. (d) Lake-level variations in Lake Van (Reimer et al., 2009). (e) Periods when the Marmara Sea and the Gemlik Gulf (base level of Lake Iznik) were lacustrine or marine (Filikci et al., 2017; Leroy et al., 2023).

Figure 10. Map showing a collection of the lowstand indicators (white dots) from the early Holocene epoch (turquoise HAR, ~10 ka cal. BP). Subfigures (a, b, c, d) are magnified images of different examples. (a, b) E–W seismic sections showing the erosive unconformity between the turquoise HAR and the underlying seismic sequence at ~66 and ~73 ms (~50 and ~55 m), respectively. (c) The N–S section shows a palaeodelta at a depth of ~73 ms (~55 m). (d) Indication of a palaeoshoreline (beach ridge) in the eastern part of the lake at ~65 ms (~49 m). The dashed turquoise line indicates the potential palaeolake level during this lowstand.

Table 1. Radiocarbon ages of the IZN19_12 and IZN21-IV sediment cores. *Calibrated ages are expressed before present, i.e., before 1950 CE. MCD denotes the master composite depth. The ages rejected for the age-model computation are in bold. #Age recalibrated from Fenn et al. (2021). **Mean age of 36 high-precision $^{40}Ar/^{39}Ar$ analyses on sanidine crystals (Çağatay et al., 2015; De Vivo et al., 2001). "mg C" refers to the quantity of carbon. The values are given by the respective laboratories, NA when no data are given.

Sediment core section	Sample name	MCD (cm)	Radiocarbon age (yr BP)*	Age cal. BP 2σ range	mg C	Type of material
IZN19_12	Poz-148250	48.5	1910 ± 30	1735 -	NA	Terr.
IZN19_12	Poz-148488	65.5	2350 ± 160	1996 -	0.03	Terr.
IZN19_12	Poz-148235	69	3410 ± 30	3569 -	NA	Terr.
IZN19_12	Poz-118215	79.5	5090 ± 40	5740 -	NA	Terr.
IZN19_12	Poz-148487	81.5	5700 ± 40	6399 -	NA	Terr.
IZN21-IV-	BE-	203.5	2506 ± 24	2493 -	0.987	Terr.
IZN21-IV-	SacA67781	263	17280 ± 120	18568 -	0.16	Terr.
IZN21-IV-	IZN21-IV-2T	305.5	/	21360 –	/	Tephra
IZN21-IV-	SacA67776	319	18030 ± 130	19507 -	0.09	Terr.
IZN21-IV-	SacA67777	436.5	19690 ± 300	21036 -	0.01	Terr.
IZN21-IV-	IZN21-IV-3T	549	/	39060 –	/	Tephra
IZN21-IV-	BE-	553.5	33945 ± 269	37883 -	0.835	Terr.
IZN21-IV-	**SacA67779**	**585**	**21970 ± 270**	**25815 -**	**0.03**	**Terr.**
IZN21-IV-	SacA68489	626	34880 ± 770	38142 -	1.16	Bulk
IZN21-IV-	SacA68490	714.5	43200 ± 2100	42905 -	1.33	Bulk
IZN21-IV-	**SacA67788**	**883.5**	**20340 ± 180**	**23953 -**	**0.08**	**Terr.**
IZN21-IV-	SacA68491	943.5	45400 ± 2800	44943 -	0.98	Bulk
IZN21-IV-	**SacA67790**	**1081.5**	**19330 ± 190**	**22965 -**	**0.05**	**Terr.**
IZN21-IV-	SacA68492	1081.5	40400 ± 1500	42128 -	1.22	Bulk

Table 2. Compilation of the HAR ages retrieved from calibrated radiocarbon ages of the three sediment cores presented in this study (IZN09/LC2&LC3, IZN19_12, and IZN21-IV). Ages in bold are considered less reliable and are therefore not considered in the following discussion. *Based on the age model from Roeser et al. (2016).

High Amplitude Reflections (HAR)	Age (ka cal. BP) IZN09/LC2&LC3*	Age (ka cal. BP) IZN19_12	Age (ka cal. BP) IZN21-IV
Turquoise (T)	~10 *	[>6.5] (hiatus)	**[4-20] (hiatus)**
Light green (LG)	22 (Y2 tephra) *	/	22 (Y2 tephra)
Dark green (DG)	**>31 (40?) ***	/	~40
Orange (O)	/	/	~45
Magenta (M)	/	/	>45 (~70)

Highlights: (maximum 85 characters, including spaces, per bullet point)

- Seismic data and sediment cores revealed Lake Iznik's past level fluctuations.

- Thirteen paleoshorelines show a stepwise transgressional phase (>45 ka cal. BP).

- Strong currents lead to contourite drift deposits from ~45 to ~10 ka cal. BP.

- A ~50m lowstand at ~10 ka cal. BP indicates a much dryer climate.

- Ongoing lake-level fluctuations due to climate, tectonics, and human impact.

Declaration of interests

☒The authors declare that they have no known competing financial interests or personal relationships that could have appeared to influence the work reported in this paper.

☐The authors declare the following financial interests/personal relationships which may be considered as potential competing interests:
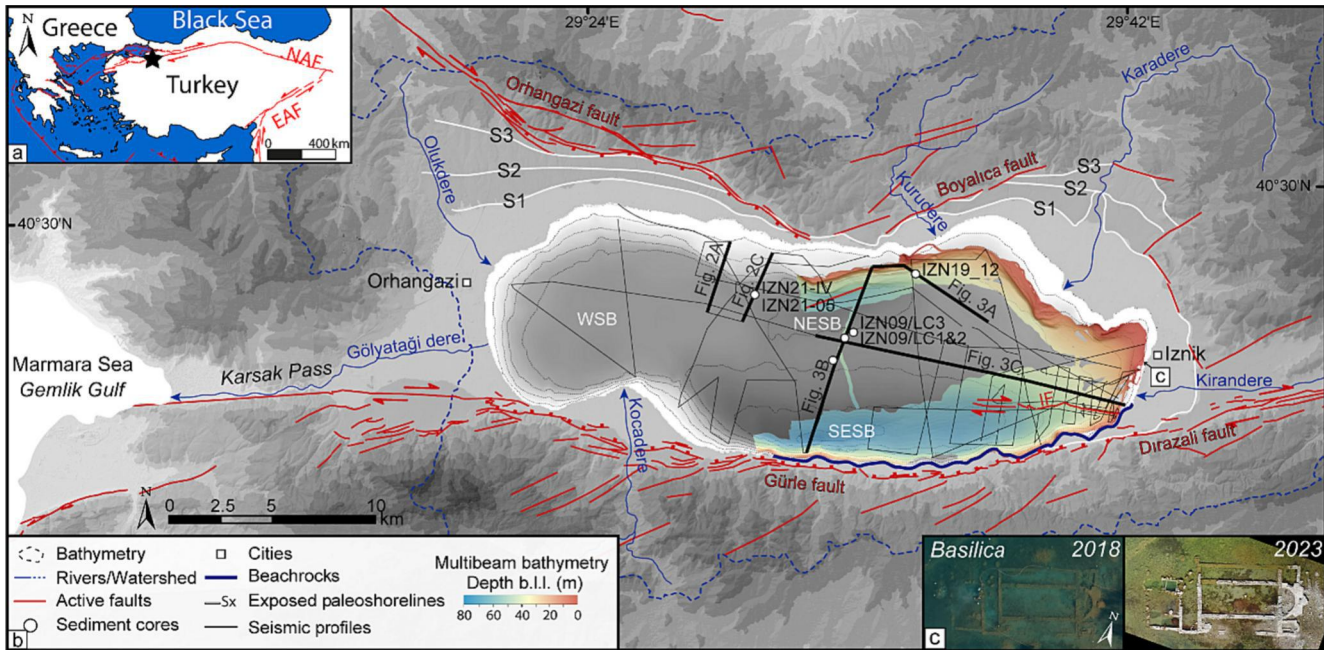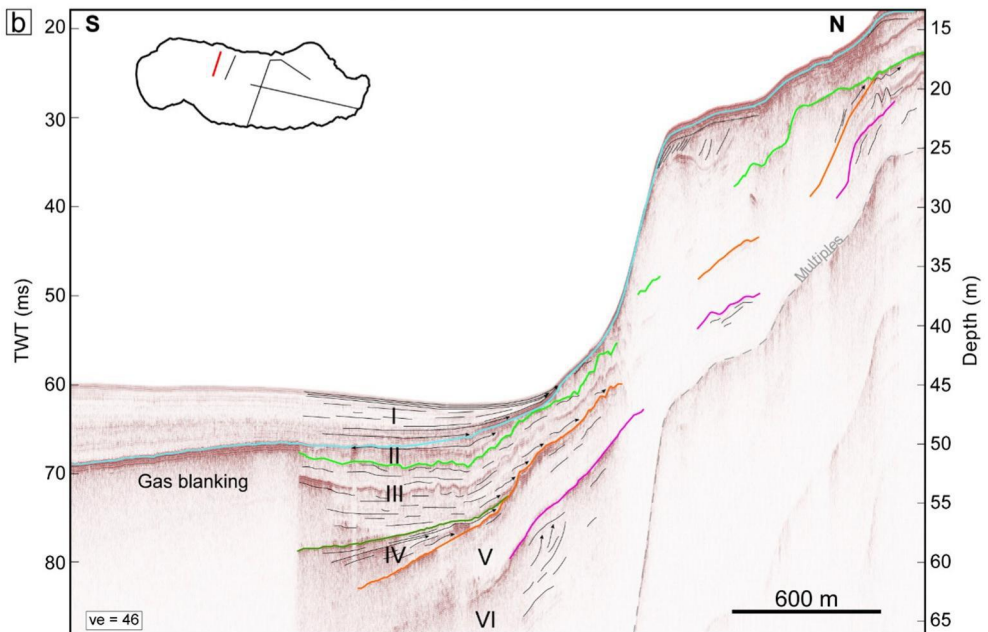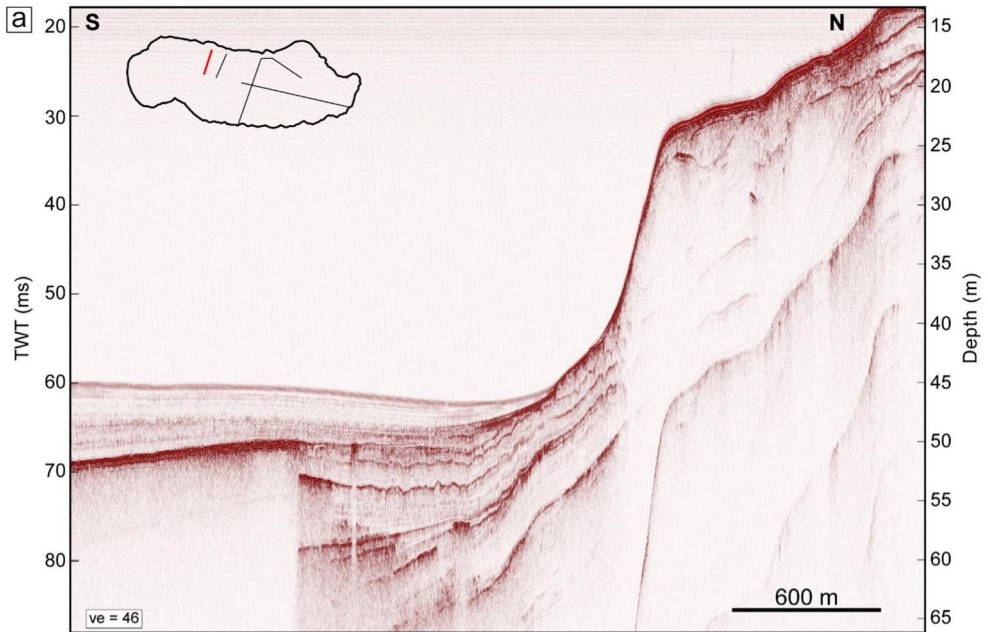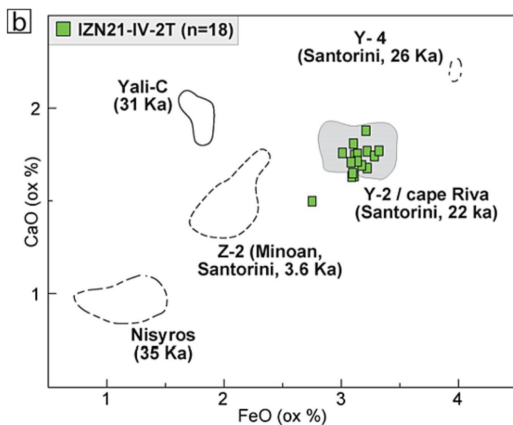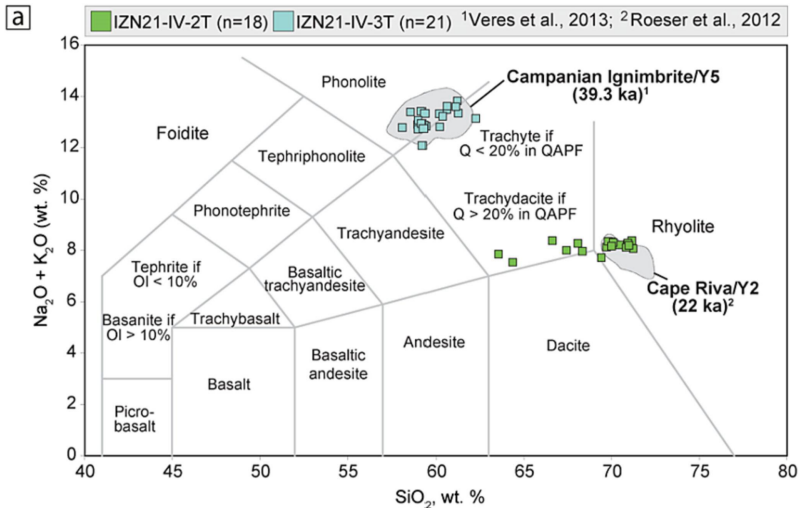
Figure 1

Figure 2AB
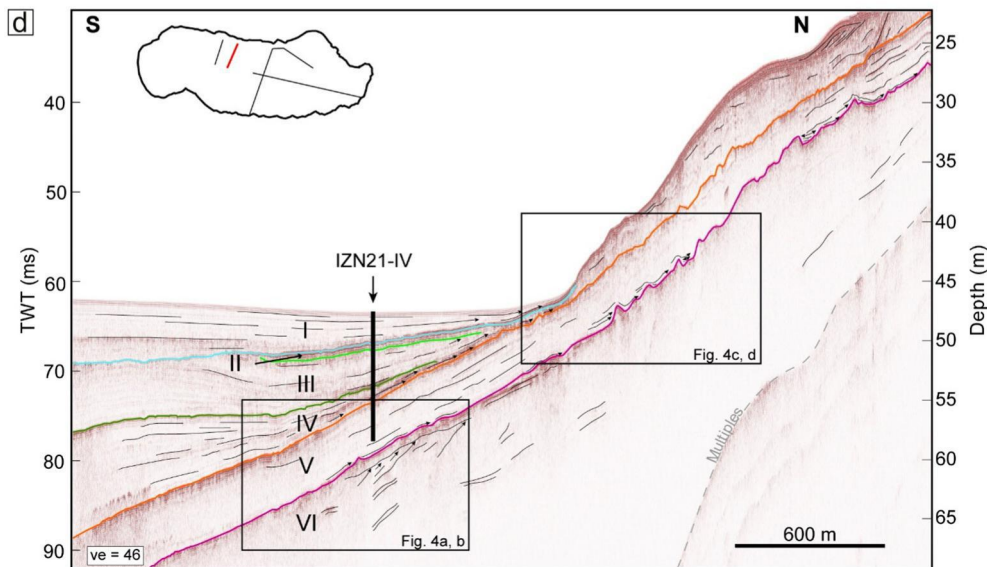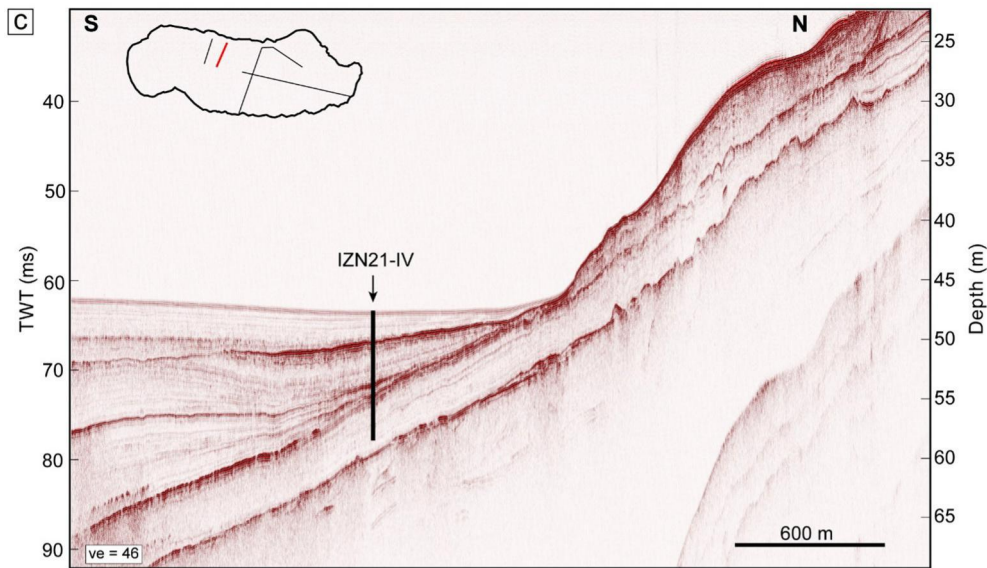
Figure 2CD
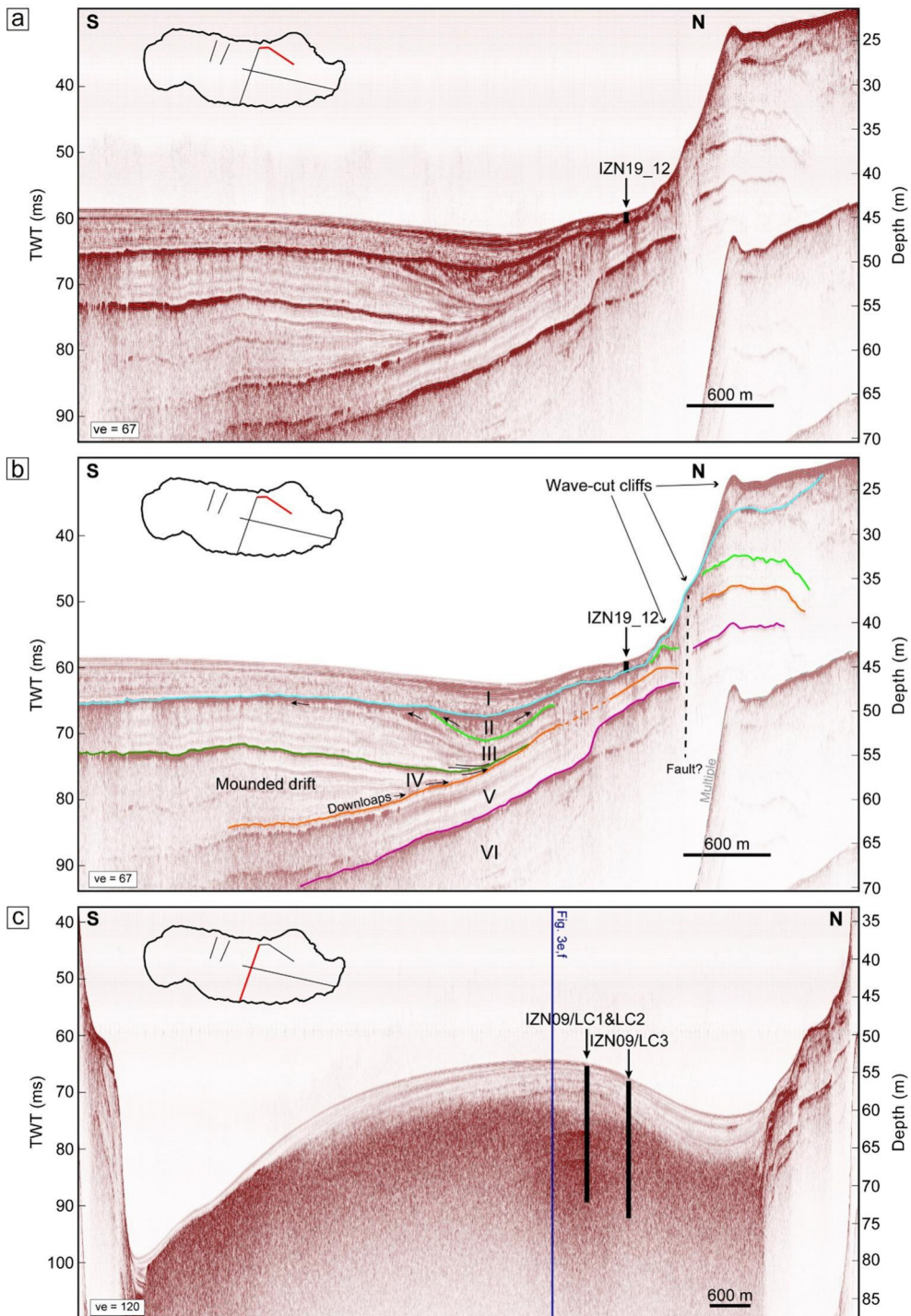
Figure 3AC
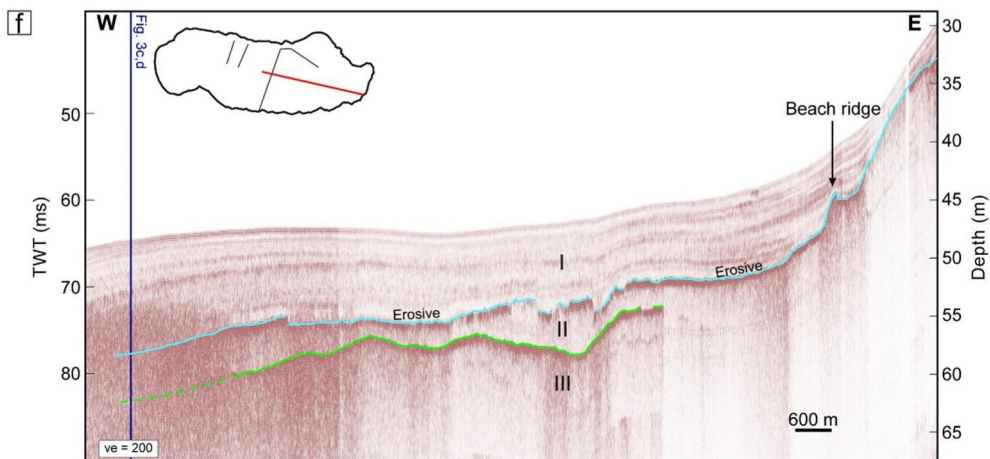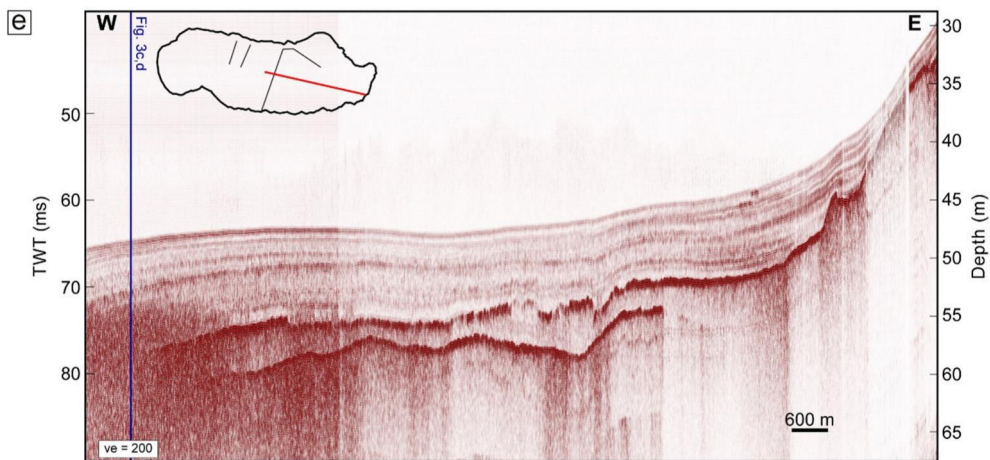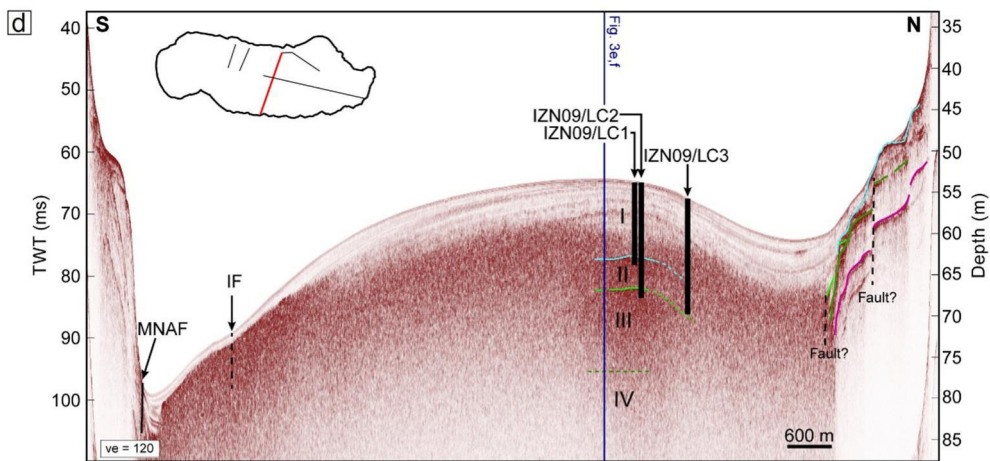
Figure 3DF
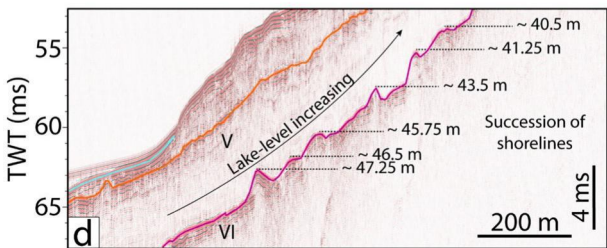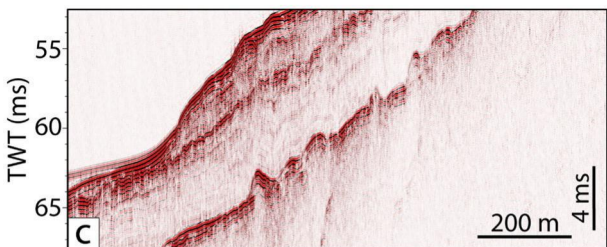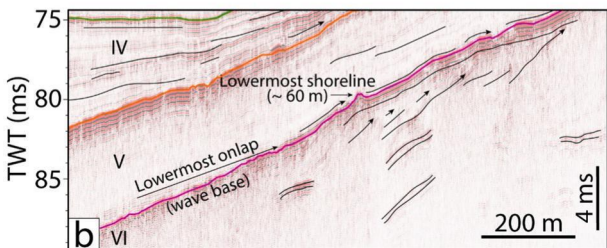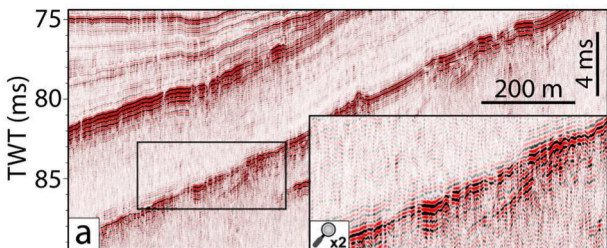
Figure 4
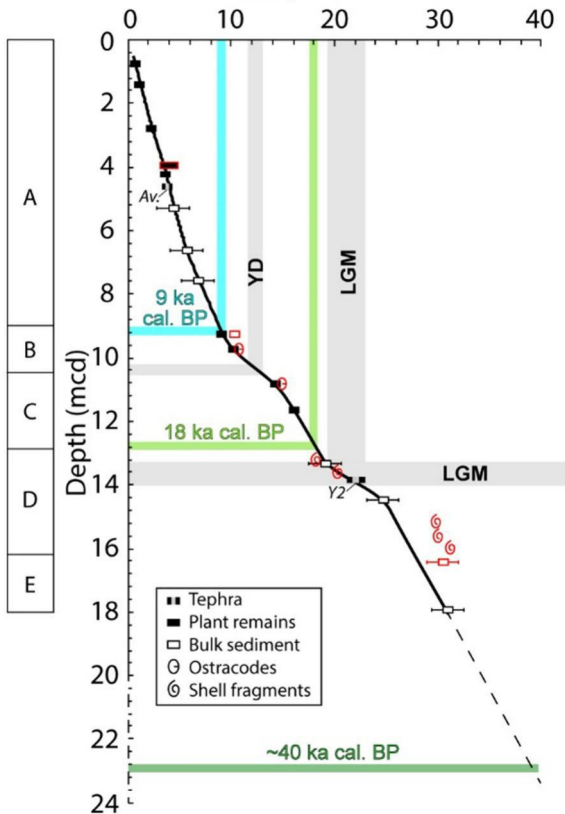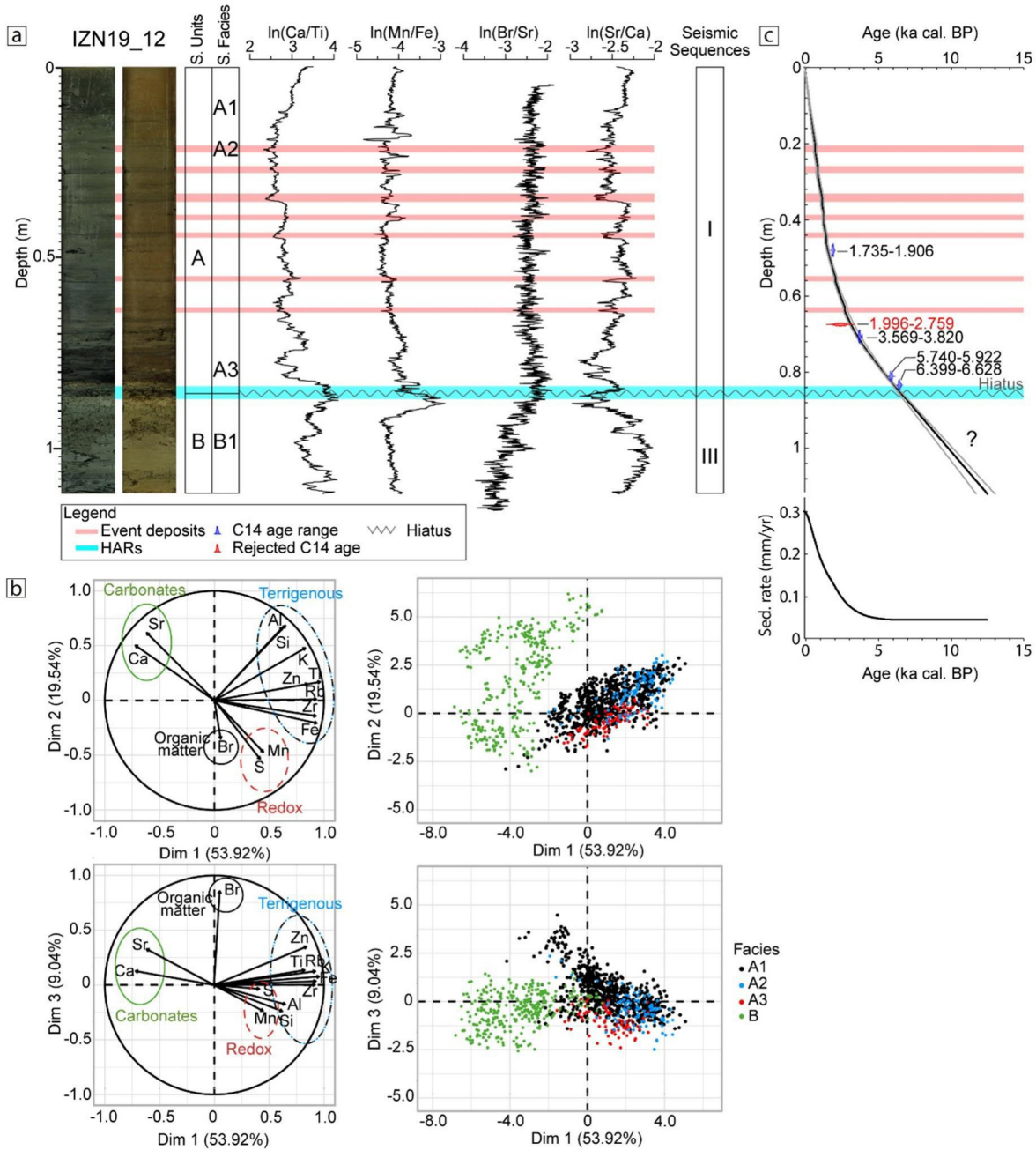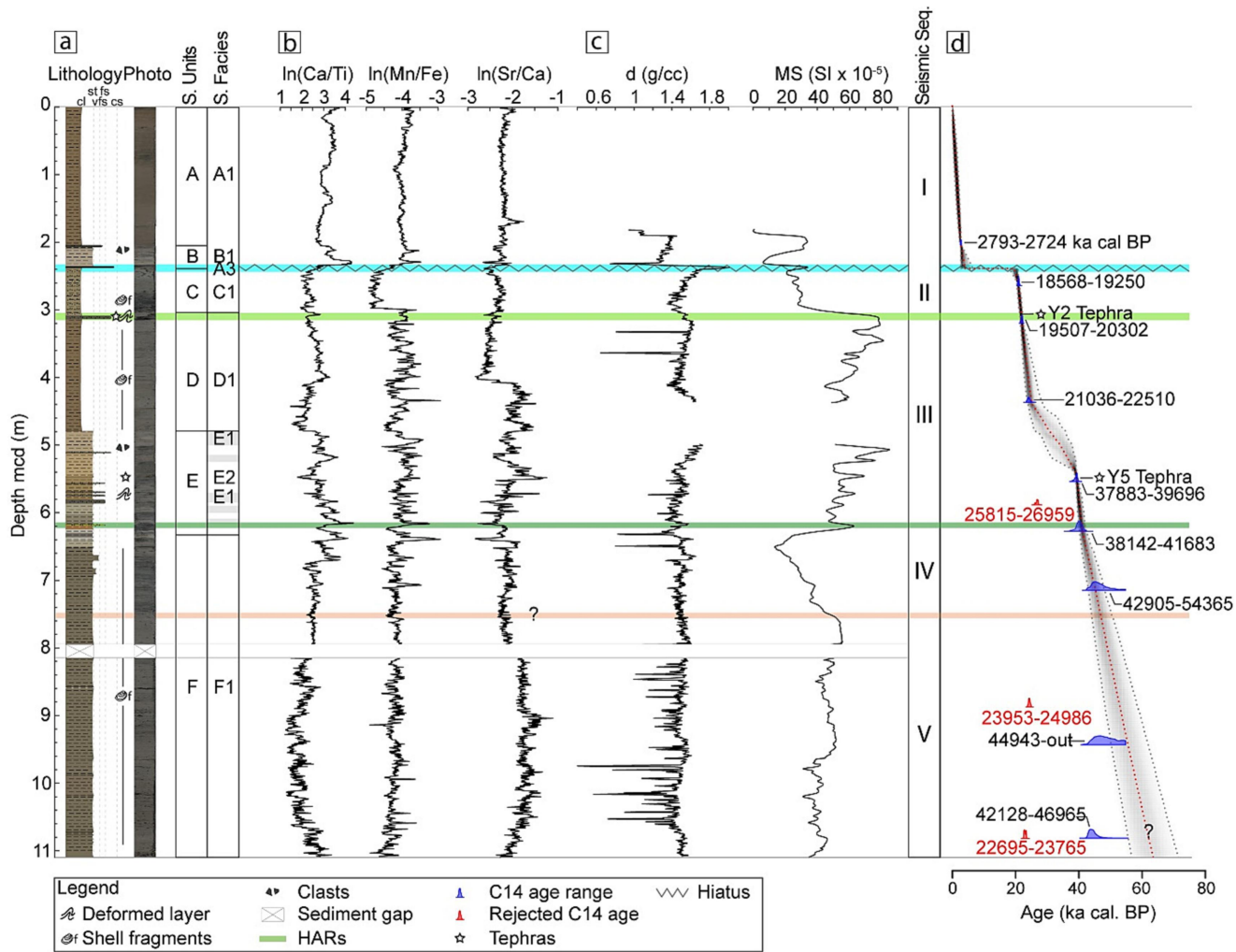
Figure 5

Figure 6

Figure 7
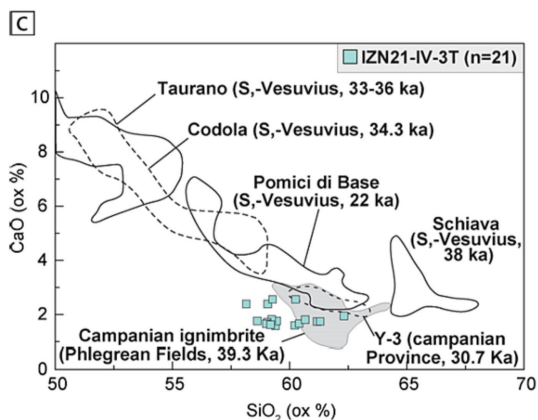
Figure 8

Figure 9

Figure 10